Wnt5b–Ryk pathway provides directional signals to regulate gastrulation movement

Shengda Lin, Lisa M. Baye, Trudi A. Westfall, and Diane C. Slusarski

Department of Biology, University of Iowa, Iowa City, IA 52242

Noncanonical Wnts are largely believed to act as permissive cues for vertebrate cell movement via Frizzled (Fz). In addition to Fz, Wnt ligands are known to regulate neurite outgrowth through an alternative receptor related to tyrosine kinase (Ryk). However, Wnt–Ryk signaling during embryogenesis is less well characterized. In this study, we report a role for Wnt5b as an instructive cue to regulate gastrulation movements through Ryk. In zebrafish, Ryk deficiency impairs Wnt5b-induced Ca^{2+} activity and directional cell movement. Wnt5b–Ryk signaling promotes polarized cell protrusions. Upon Wnt5b stimulation, Fz2 but not Ryk recruits Dishevelled to the cell membrane, suggesting that Fz2 and Ryk mediate separate pathways. Using co-culture assays to generate directional Wnt5b cues, we demonstrate that Ryk-expressing cells migrate away from the Wnt5b source. We conclude that full-length Ryk conveys Wnt5b signals in a directional manner during gastrulation.

Introduction

Zebrafish gastrulation is characterized by directional cell migration toward the midline, resulting in the narrowing/lengthening of tissues known as convergent extension (CE; Solnica-Krezel, 2005). β-Catenin–independent, or noncanonical, Wnt signaling is pivotal in vertebrate CE (Rohde and Heisenberg, 2007). In *Drosophila melanogaster*, the planar cell polarity (PCP) pathway establishes polarity in epithelial cells (Zallen, 2007). Despite shared core components (Zallen, 2007), noncanonical Wnt activities in vertebrates are not fully explained by the mechanisms of *Drosophila* PCP. Unlike *Drosophila* epithelia, vertebrate mesenchyme possesses different physiological traits and dynamic cell behaviors such as directional migration, as well as planar and radial cell intercalations (Yin et al., 2008). Moreover, *Drosophila* Wnt mutants do not exhibit PCP phenotypes, whereas zebrafish Wnt mutants (*wnt5b/pipetail* and *wnt11/silberblick*) have cell movement defects (Solnica-Krezel, 2005). Because *wnt5b* and *wnt11* RNAs rescue the *wnt11* genetic mutant (Heisenberg et al., 2000; Kilian et al., 2003), noncanonical Wnts are largely believed to have a permissive role in CE. However, zygotic loss of *wnt5b/pipetail* displays severe CE defects (Rauch et al., 1997) and cannot be rescued by exogenous *wnt5b* RNA (Kilian et al., 2003; Westfall et al., 2003a), suggesting that Wnt5 signaling may be both permissive and instructive. Receptor tyrosine kinases (RTKs), including related to tyrosine kinase (Ryk), are Wnt responsive (Cadigan and Liu, 2006; Nusse, 2008). In fact, both *Drosophila* Wnt5 and vertebrate Wnt5a act as repulsive cues to Ryk-expressing neurons (Yoshikawa et al., 2001; Liu et al., 2005; Keeble and Cooper, 2006; Keeble et al., 2006). We hypothesize that a Wnt-dependent mechanism is used in concert with the conserved PCP framework to coordinate precise vertebrate CE movements.

Ryk protein is composed of an extracellular domain (ECD) similar to the secreted Wif-1 (Wnt inhibitory factor 1), a transmembrane (TM) domain, and a kinase-dead tyrosine kinase domain (Halford and Stacker, 2001) and can bind to Wnt5a protein (Yoshikawa et al., 2003; Liu et al., 2005; Keeble et al., 2006; Kim et al., 2008). Diverse molecular events downstream of Ryk include heterodimerization with other RTKs (Halford et al., 2000), src kinase activation (Wouda et al., 2008), and Frizzled (Fz) binding (Lu et al., 2004; Kim et al., 2008), and additionally, Wnt induces the nuclear translocation of the Ryk

Correspondence to Diane C. Slusarski: diane-slusarski@uiowa.edu

Abbreviations used in this paper: CE, convergent extension; dpf, day postfertilization; Dvl, Dishevelled; ECD, extracellular domain; EVL, enveloping layer; Fz, Frizzled; hpf, hour postfertilization; ICD, intracellular domain; IPL, inner plexiform layer; IRES, internal ribosome entry site; MO, morpholino oligonucleotide; PCP, planar cell polarity; RTK, receptor tyrosine kinase; Ryk, related to tyrosine kinase; TM, transmembrane; UTR, untranslated region; YSL, yolk syncytial layer.

The Rockefeller University Press $30.00
J. Cell Biol. Vol. 190 No. 2 263–278
www.jcb.org/cgi/doi/10.1083/jcb.200912128

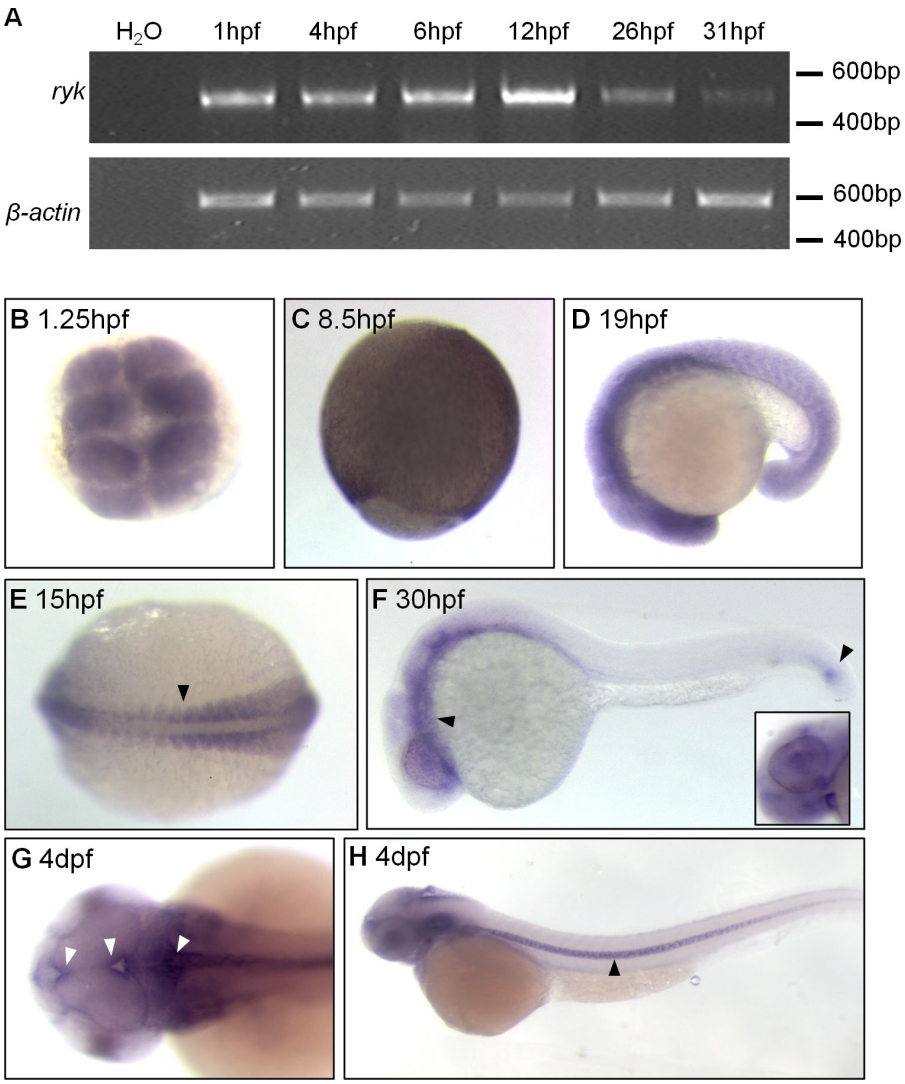

Figure 1. **Zebrafish *ryk* expression profile.** (A) Semiquantitative RT-PCR showing temporal *ryk* expression. (B–E) Whole-mount in situ hybridization reveals ubiquitous *ryk* expression throughout maternal (B) and gastrula stages (C–E) with enrichment in somites (E, arrowhead) and the central nervous system. (F) At 30 hpf, *ryk* is expressed in the brain and tail (arrowheads) and notably the eyes (inset). (G and H) At 4 dpf, *ryk* is expressed in the lining of ventricular zones (G, arrowheads) and notochord (H, arrowhead). Stages and orientation: 1.25 hpf, animal pole view; 8.5 hpf, lateral view; 15 hpf, dorsal view with anterior to the left; 19 and 30 hpf, lateral view with anterior to the left; 4 dpf, dorsal view of brain and lateral view of the whole body, anterior to the left.

intracellular domain (ICD) to promote neuronal differentiation (Lyu et al., 2008).

Ryk signaling has been shown to be independent of Fz, as well as facilitating Fz activity. In *Caenorhabditis elegans*, Ryk is necessary to polarize vulval cells, and genetic analysis indicates that Ryk and Fz are involved in separate pathways (Inoue et al., 2004; Green et al., 2008). Ryk and Fz have opposing roles in Wnt5-mediated *Drosophila* salivary gland migration (Harris and Beckendorf, 2007) and Wnt3a-mediated retinal ganglion cell axon outgrowth in chick and mouse (Schmitt et al., 2006). In contrast, Ryk synergizes with Fz to facilitate Fz-dependent signaling in *Xenopus laevis* (Kim et al., 2008) and 293T cells (Lu et al., 2004). Knockdown of *Xenopus* Ryk results in gastrulation defects with compromised Wnt11-induced Fz7 and Dishevelled (Dvl) endocytosis (Kim et al., 2008). In zebrafish, Wnt11 does not induce Fz7/Dvl endocytosis, but rather stimulates Fz7/Dvl accumulation on the plasma membrane (Witzel et al., 2006), raising the possibility that Wnt–Ryk and Wnt–Fz signaling pathways are distinct.

We find that Ryk deficiency in zebrafish leads to gastrulation defects and that Ryk acts downstream of Wnt5b to regulate directional cell movement. Consistent with these observations, we show that Wnt5b binds to Ryk and Ryk function is necessary to modulate Wnt5b-induced Ca^{2+} dynamics. We also show that Wnt5b and Ryk knockdown embryos (morphants) share similar defects relative to cell movement and neuronal migration. Ryk is internalized, and Ryk-expressing cells show increased cellular protrusions in a Wnt5b-dependent manner. Co-culture of zebrafish animal caps demonstrates that Wnt5b acts as an instructive cue. In this assay, Wnt5b-expressing cells and Fz2-expressing cells show extensive intermingling; in contrast, Wnt5b- and Ryk-expressing cells demonstrate restrictive intermingling, and Ryk cells show directed migration away from the Wnt5b source. We find that Fz2 but not Ryk recruits Dvl to discrete domains on the plasma membrane, similar to previously reported Wnt11–Fz7 interactions (Witzel et al., 2006) and consistent with our working model that Wnt5–Ryk and Wnt5–Fz lead to distinct signaling outputs. Our findings demonstrate that noncanonical Wnt signaling modulates zebrafish cell movement via two separate mechanisms: activating the core PCP components to establish cellular polarity (Simons and Mlodzik, 2008) and Ryk-mediated signaling to regulate directional cell migration.

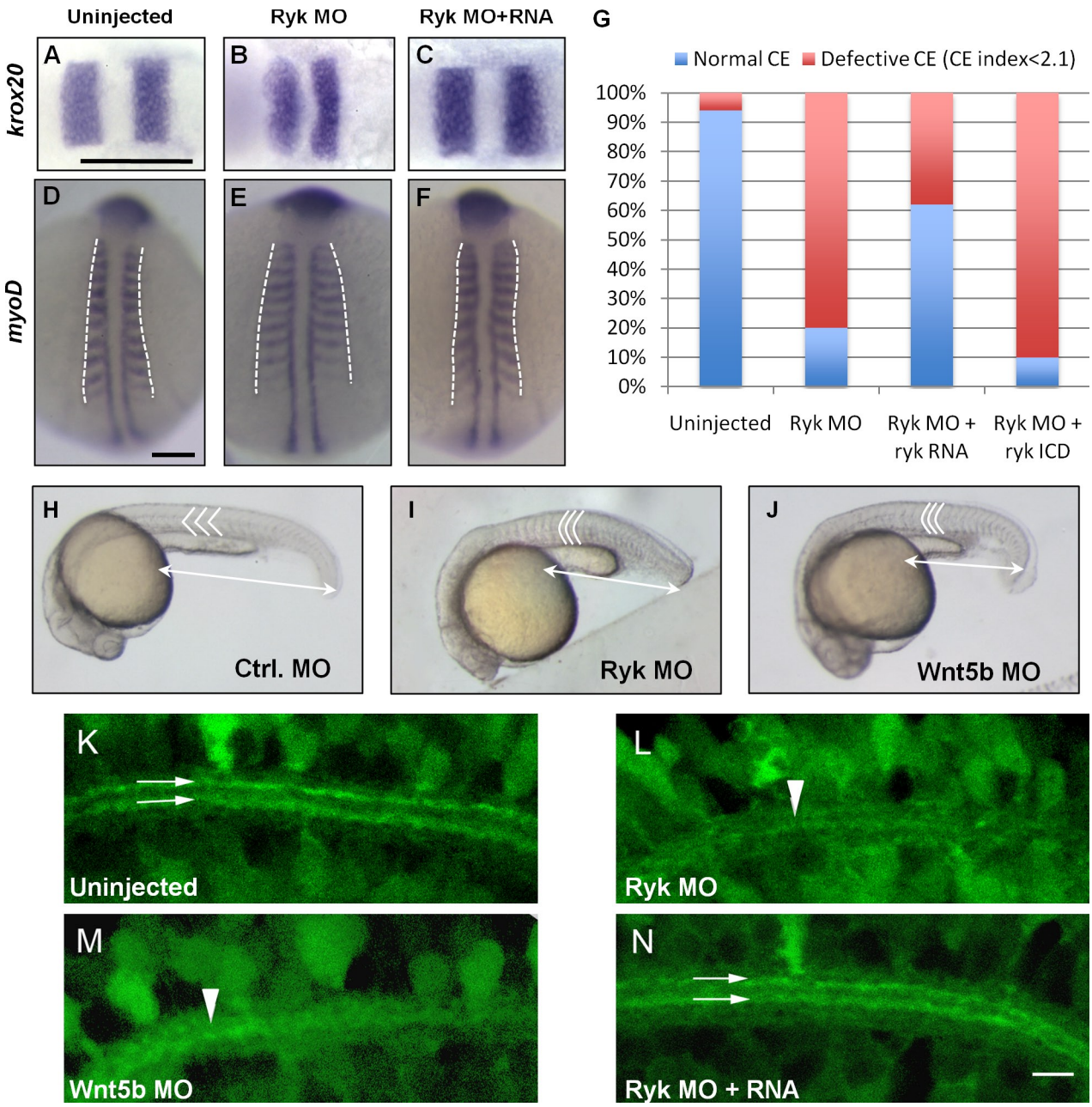

Figure 2. **Zebrafish *ryk* loss of function phenotype.** (A–F) Evaluating CE with markers. Dorsal view, anterior to the left of *krox20* expression in uninjected (A), Ryk MO–injected (B), and Ryk MO co-injected with *ryk* RNA (C) embryos. Dorsal view, anterior to the top of *myoD* expression in uninjected (D; *n* = 32), Ryk MO–injected (E; *n* = 25), and Ryk MO co-injected with *ryk* RNA (F; *n* = 29) embryos. (D–F) The white dashed lines outline the lateral border of *myoD* domains. (G) Quantification of the CE phenotype, including embryos co-injected with Ryk MO and *ryk* ICD RNA (*n* = 30; 2.0 pmol Ryk MO; 50 pg *ryk* RNA; 50 pg *ryk* ICD RNA). Columns display the percentage of embryos at 10–11-somite stage with normal or defective CE index. (H–J) Morphological phenotypes at 24 hpf. Control (Ctrl.) MO–injected embryos (H) with even-spaced, V-shaped somites and Ryk MO (I)–, and Wnt5b MO–injected (J) embryos with reduced posterior A–P axis (double-headed arrow), and curved, tightly packed somites (white lines). Lateral view with anterior to the left. (K–N) Transverse central retina confocal images of 3-dpf *huc*:GFP transgenic embryos. Control (K) and Ryk MO (L)–, Wnt5b MO (M)–, and Ryk MO with *ryk* RNA (N)–injected embryos. The two organized sublaminae in the wild-type IPL (K, arrows) are less organized in both the Wnt5b (M, arrowhead) and Ryk (L, arrowhead) morphants. *ryk* RNA co-injection partially rescues Ryk MO–induced phenotype (N, arrows). Bars: (A–F) 150 µm; (K–N) 5 µm.

Results

Zebrafish Ryk cloning and expression pattern

Zebrafish *ryk* exists as a single-copy gene (Ensembl assembly release 55) and the ~1-Mb flanking sequences show synteny with the corresponding region in the human genome (Fig. S1 A). Zebrafish Ryk protein is 604 aa in length and 76% identical to its human homologue (Fig. S1 B). RT-PCR and whole-mount in situ hybridization demonstrate zebrafish *ryk* expression at maternal and zygotic stages (Fig. 1). During somite stages, *ryk* is enriched in the developing somites and central nervous system (Fig. 1, D and E). After 30 h postfertilization (hpf), *ryk* is highly expressed in the brain, heart, eyes, and the posterior tail (Fig. 1, F

and inset). At 4 d postfertilization (dpf), *ryk* shows enriched expression in the lining of the ventricular zones and in the notochord (Fig. 1, G and H).

Overlapping phenotypes with Ryk and Wnt5b knockdown

To evaluate the developmental role of *ryk*, gene knockdown was performed with translation-blocking antisense morpholino oligonucleotides (MOs). Ryk MO injection resulted in shortened anterior–posterior (A–P) body axis. Compared with control (Fig. 2, A and D), Ryk MO–injected embryos had reduced distance between rhombomeres 3 and 5 of the hindbrain (*krox20*), and the somites of the trunk (*myoD*) showed lateral expansion (Fig. 2, B and E). A–P extension can be represented by the length to width ratio of the *myoD* domain as a CE index value for analysis (Angers et al., 2006). Wild-type embryos show a CE index >2.5 (Fig. 2 D, dashed lines). Embryos with a CE index <2.1 are considered CE defective. Using this parameter, Ryk knockdown resulted in >80% CE-defective embryos. Co-injection of Ryk MO and MO-resistant *ryk* RNA at a subphenotypic dose (50 ng; Fig. S2 C) was sufficient to suppress the CE defect (Fig. 2, C and F) to only 38% (Fig. 2 G). MO specificity was confirmed by co-injection of Ryk MO with a reporter construct (*ryk* 5′ untranslated region [UTR] containing the MO target sequence fused to EGFP), resulting in diminished EGFP expression (Fig. S2 A), and also by generating similar phenotypes with a second Ryk MO (Fig. S2 B).

Consistent with the hypothesis that Ryk functions as a Wnt5b receptor is the strikingly similar phenotypes of Ryk and Wnt5b morphants. Morphological analysis shows a characteristic reduced posterior extension and tightly packed somites (Fig. 2, I and J), compared with control (Fig. 2 H). Both *ryk* (Fig. 1 F, inset) and *wnt5b* (not depicted) are expressed in the retina. The *huc*:GFP transgenic line (Park et al., 2000), in which cytoplasmic GFP highlights ganglion and amacrine cell neurite outgrowth and lamina formation, was used to determine whether Wnt5b and Ryk have overlapping function in the retina. The inner plexiform layer (IPL) of the retina harbors synaptic connections between the ganglion, amacrine, and bipolar cells. At 3 dpf, *huc*:GFP transgenic embryos had two distinct sublaminae within the IPL (Fig. 2 K, arrows); however, in Wnt5b MO (Fig. 2 M)– and Ryk MO (Fig. 2 L)–injected embryos, these sublaminae were not well defined, suggesting a disruption in neurite outgrowth. This phenotype can be partially rescued by co-injection of *ryk* RNA with Ryk MO (Fig. 2 N). Thus, Ryk and Wnt5b knockdown show overlapping defects relative to CE and retina structure.

To evaluate genetic interaction between Wnt5b and Ryk, we performed double knockdown and determined the length to width ratio, CE index (Fig. 3). At the 13–14-somite stage, normal CE had an index of 2.8 and higher. Mild CE defects had an index between 2.1 and 2.8, and severe phenotypes had a CE index <2.1. Controls showed normal A–P axis extension with a CE index >2.8 (Fig. 3, A and E). Individually, low-dose Wnt5b MO (0.5 pmol) or low-dose Ryk MO (1.0 pmol) generated mild CE defects (89% and 93% of embryos, respectively; Fig. 3, B, C, and E). For co-injection, MO doses were reduced by half

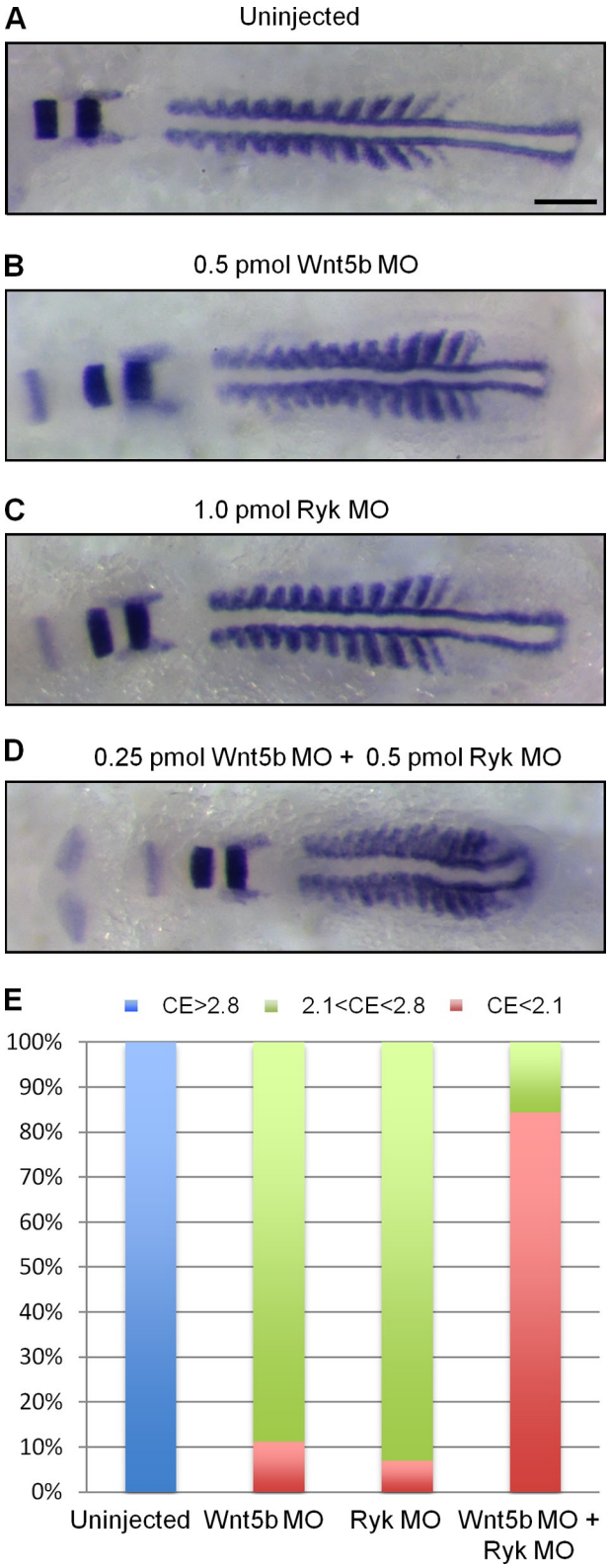

Figure 3. **Wnt5b and Ryk show synergistic effects in zebrafish CE.** (A–D) In situ hybridization with combined *myoD*, *krox20*, and *pax2a* probes. Dorsal view, anterior to the left of control (A) and low-dose Wnt5b MO (0.5 pmol; B)–, low-dose Ryk MO (1.0 pmol; C)–, and combined Wnt5b MO (0.25 pmol) and Ryk MO (0.5 pmol; D)–injected embryos. (E) Quantification of CE index defects. Bar, 150 µm.

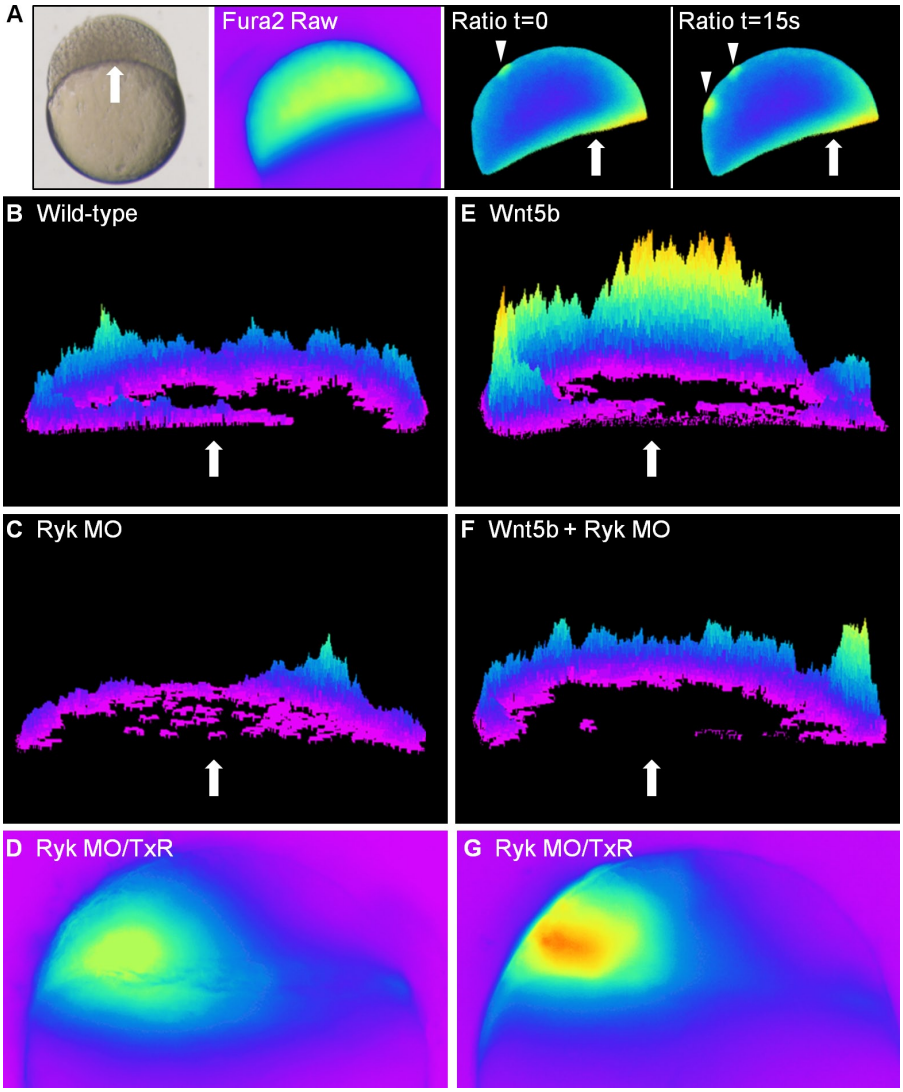

Figure 4. **Wnt5b–Ryk modulation of Ca^{2+} release.** (A) Analyzing Ca^{2+} release in zebrafish blastula/epiboly stage embryos. Ca^{2+} detected by Fura-2 ratiometric dye. Sample ratio images collected at 15-s intervals with time t = 0 s compared with t = 15 s showing examples of Ca^{2+} release events in the EVL (arrowheads) and YSL (arrows). (B–D) Ryk knockdown blocks endogenous Ca^{2+} release. (B) Endogenous Ca^{2+} release in control embryo (Video 1). (C and D) Unilateral injection of Ryk MO reduced endogenous Ca^{2+} activity (C; Video 2); lineage tracer Texas red (TxR) co-mixed with Ryk MO reveals the injected side (D). (E–G) Ryk deficiency blocks Wnt5b-induced Ca^{2+} release. (E) Wnt5b injection activates Ca^{2+} release (Video 3). (F and G) Unilateral injection of Ryk MO suppressed Wnt5b-induced activation (F; Video 4); lineage tracer indicates the injected side (G). Arrows note the YSL.

(0.25 pmol Wnt5b MO + 0.5 pmol Ryk MO). All embryos injected with combined MOs presented CE defects, with the majority (84%) showing severe CE defects and only 16% showing mild CE defects comparable with single knockdown (Fig. 3, D and E). We thereby conclude that Wnt5b and Ryk function synergistically to regulate zebrafish CE movement.

Ryk acts downstream of Wnt5b

Wnt5 is sufficient to activate Ca^{2+} release, and zygotic *wnt5b/pipetail* embryos show reduced Ca^{2+} release (Slusarski et al., 1997b; Westfall et al., 2003a; Freisinger et al., 2008). Using Ca^{2+} release as a physiological readout for Wnt5b activity, we tested the impact of Ryk function on endogenous and Wnt5b-induced Ca^{2+} release dynamics in vivo. Embryos injected with Fura-2 ratiometric Ca^{2+} sensor and imaged at early stages of epiboly demonstrated the most notable endogenous Ca^{2+} release dynamics in the enveloping layer (EVL) and yolk syncytial layer (YSL; Fig. 4 A; arrowheads point to the EVL, and arrows point to the YSL; Westfall et al., 2003a). A time course of ratio images was collected, aligned, and subjected to a subtractive algorithm to identify changes in free Ca^{2+} levels at 15-s intervals (Fig. 4 A). Changes in Ca^{2+} release dynamics are represented as a color scale surface plot showing the total number of events relative to the location in the embryo (Fig. 4, B–G; Slusarski and Corces, 2000; Freisinger et al., 2008). In wild-type embryos, we observed a characteristic frequency and distribution of endogenous Ca^{2+} release (Fig. 4 B and Video 1). Unilateral injection of Ryk MO co-mixed with lineage tracer Texas red (Fig. 4 D) resulted in reduced endogenous activity on the injected side (Fig. 4 C and Video 2). Because expression of Wnt5b in zebrafish embryos is sufficient to activate Ca^{2+} release (Fig. 4 E and Video 3), we tested whether Ryk activity is necessary for Wnt5b-induced Ca^{2+} release. Embryos were injected at the one-cell stage with *wnt5b* RNA and Fura-2 for uniform expression. At the 16–32-cell stage, Ryk MO co-mixed with lineage tracer was injected unilaterally into a subset of cells (Fig. 4 G). Knockdown of Ryk was sufficient to suppress Wnt5b-induced Ca^{2+} release (Fig. 4 F and Video 4). This impact on Ca^{2+} dynamics indicates that Ryk functions downstream of Wnt5b.

Wnt5b–Ryk interaction mediates morphological changes

To define a role for Ryk function and address the impact of Wnt5b–Ryk interaction on gastrula cell migration, we performed

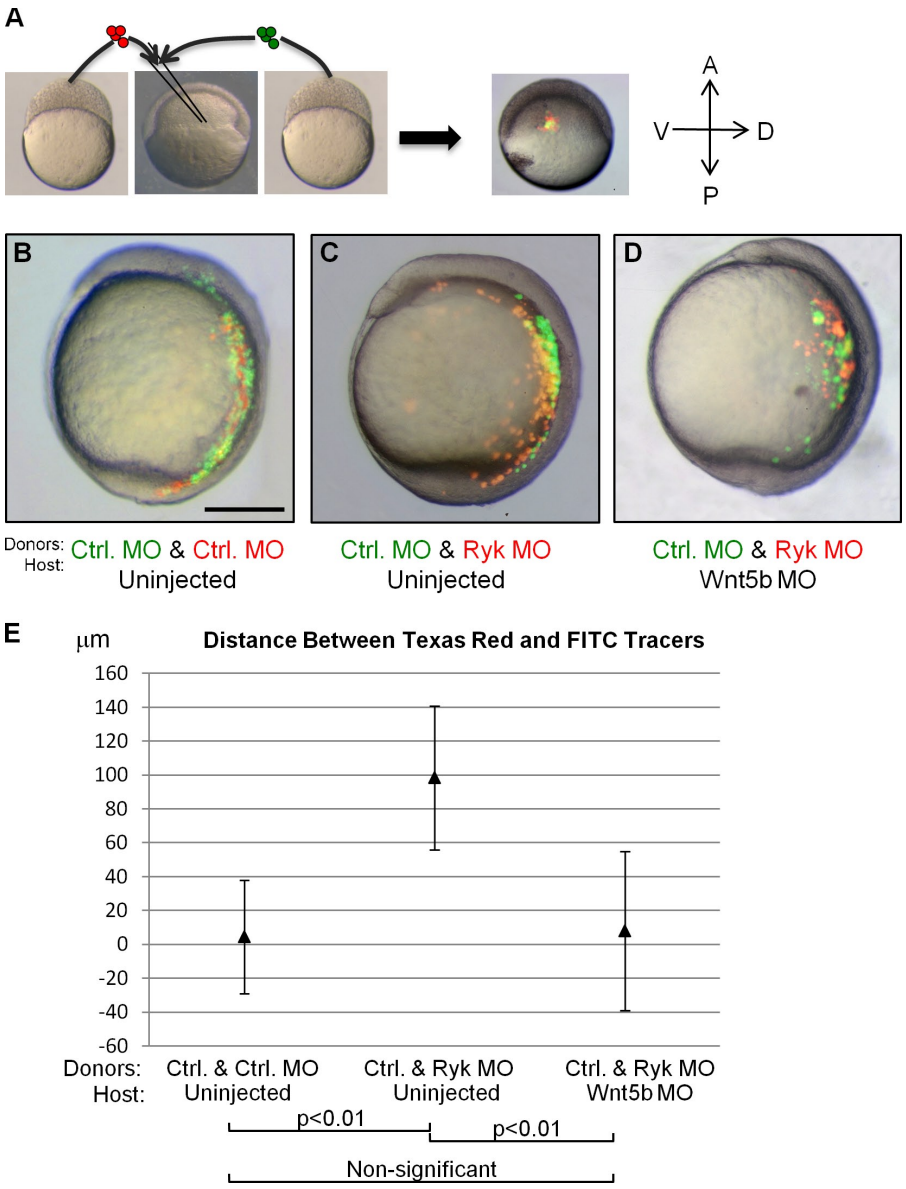

Figure 5. **Ryk deficiency leads to directional cell migration defects in a Wnt5b-dependent manner.** (A–D) Assessment of cell migration. Donor cells separately labeled with FITC (green) or Texas red (red) were transplanted into the center of the lateral mesoderm at the germ ring margin (A). Uninjected host with control (Ctrl.) MO–injected (red and green) donor cells (B); uninjected host with control MO–injected (green) and Ryk MO–injected (red) donor cells (C); Wnt5b MO–injected host with control MO–injected (green) and Ryk MO–injected (red) donor cells (D). (E) Quantification of the mean distance between green and red tracers. 10 embryos were scored for each group, and error bars represent standard deviation. One-way analysis of variance and Tukey's honestly significant difference test were used to determine statistical significance. Bar, 250 µm.

a series of transplantation assays. Before transplantation, two donor embryos were injected with control MO combined with fluorescent lineage marker. At ∼3 hpf, donor cells were mixed and transplanted into the lateral mesoderm at the germ ring margin of a shield-stage host (∼6 hpf; Fig. 5 A). Cells in this region of the embryo migrate in a ventral to dorsal direction and extend in both anterior and posterior directions. The distribution of transplanted cells was scored after host embryos completed gastrulation (∼10 hpf). Transplanted cells from two control MO–injected donors (red and green) demonstrated similar convergent movement (Fig. 5 B). In contrast, Ryk MO–injected cells (red) demonstrated markedly reduced convergent movement compared with control MO–injected cells (green; Fig. 5 C). When Ryk MO (red) and control MO (green) cells were transplanted into Wnt5b knockdown host embryos, both control MO and Ryk MO cells showed reduced dorsal convergence (Fig. 5 D). To quantify cell migration between the two populations of transplanted cells, the distance from the center of the embryo was averaged for red- and green-labeled cells (Fig. 5 E). In wild-type hosts, the mean difference in mean position of Ryk MO–injected cells (red) compared with control MO–injected cells (green) was 100 µm, corresponding to 5–10 cells, and was statistically different from the control group ($P < 0.01$; Fig. 5 E). In contrast, there was no significant difference in mean distance traveled by Ryk MO and control MO cells transplanted into Wnt5b knockdown hosts (Fig. 5 E). These data indicate that dorsal convergence is compromised in the absence of Ryk and in the absence of the Wnt5b ligand, either with or without the Ryk receptor.

Wnt5b–Ryk interaction was evaluated in individual cells with tagged constructs. mCherry-tagged Ryk (Ryk-mCherry) showed ubiquitous membrane localization at 90% epiboly (Fig. S3 A). Donor embryos were also injected with Wnt5b MO to reduce effects caused by autocrine signaling and did not alter cell shape or the membrane localization in Ryk-mCherry–expressing cells (Fig. 6 A). Wnt5b-expressing cells were traced by membrane EGFP driven by an internal ribosome entry site (IRES) in a Wnt5b-IRES-EGFP-CAAX construct (Fig. 6 B). Ryk-mCherry donor cells transplanted into a Wnt5b-IRES-EGFP-CAAX host

displaced redistribution of mCherry signals away from the membrane (Fig. 6, C and F). Colocalization of Ryk-mCherry with Caveolin1-EGFP indicates that Ryk redistribution is caused by internalization (Fig. S3, D and E). Moreover, Wnt5b induced Ryk-mCherry cells to undergo significant shape changes with increased filopodia and lamellipodia-like protrusions (Fig. 6, C and F). To determine whether these changes require Wnt5b, Ryk-mCherry donor cells were transplanted into Wnt5b MO + EGFP-CAAX–injected host embryos, and no obvious morphological change in Ryk-expressing cells was observed (Fig. 6 D). In addition, donor cells expressing a dominant-negative Ryk (lacking the ICD; dnRyk-mCherry) demonstrate no morphological changes when transplanted into Wnt5b-IRES-EGFP-CAAX–expressing host (Fig. 6 E).

Quantification of cell shape changes was used to demonstrate increased cell roundness in *wnt5b/pipetail* mutants (Kilian et al., 2003). Measuring transplanted cells revealed that dnRyk-expressing cells in Wnt5b-expressing host (0.77 ± 0.01; group 1), Ryk-expressing cells in Wnt5b-depleted host (0.76 ± 0.02; group 2), and control cells in Wnt5b-depleted host (0.73 ± 0.02; group 3) all show similar cell roundness (Fig. 6, G and H). In contrast, Ryk-expressing cells, transplanted into a Wnt5b-expressing host show significantly reduced mean cell roundness (0.53 ± 0.03; group 4) in a wide distribution (Fig. 6, G and I). Collectively, our data indicate that Wnt5b stimulates the protrusive activity of Ryk-expressing cells in zebrafish gastrula.

Fz2 and Ryk demonstrate distinct responses to Wnt5b

Because Ryk signaling has been shown to both be distinct from Fz (Inoue et al., 2004; Schmitt et al., 2006; Harris and Beckendorf, 2007) as well as facilitate Fz signaling (Lu et al., 2004; Kim et al., 2008) in different models, we also evaluated Fz protein distribution in response to Wnt5b activation in zebrafish. In vivo imaging of Fz2-mCherry–expressing cells showed predominantly membrane localization in donor embryos (Fig. S3 B). When transplanted into Wnt5b-expressing hosts, Fz2-mCherry maintained membrane localization (Fig. S3 C, arrowheads), and cell shape did not change.

Because Fz is known to recruit Dvl to the cell membrane (Zallen, 2007), we next determined the extent that Ryk and Fz influence Dvl membrane localization. We used mosaic injections to analyze receptor and Dvl distribution relative to Wnt5b stimulation. At the 8–16-cell stage, one cell of an embryo was injected with Fz2-mCherry co-mixed with Dvl-EGFP, and an adjacent cell was injected with Wnt5b-IRES-nls-EGFP (Fig. 7 A) and imaged at the 90% epiboly stage. When adjacent to Wnt5b-expressing cells, Dvl-EGFP and Fz2-mCherry colocalized in discrete domains on the plasma membrane (Fig. 7, B–D). A majority of Dvl-EGFP–positive areas also showed Fz2-mCherry localization (90 ± 3%; Fig. 7 K). To determine whether Ryk activity was necessary for Fz2 and Dvl colocalization, Ryk MO was co-injected with Dvl-EGFP and Fz2-mCherry. Ryk deficiency did not compromise Dvl-EGFP and Fz2-mCherry colocalization (Fig. 7, E–G), as 95 ± 2% of the Dvl-EGFP–positive area also displayed Fz2-mCherry localization (Fig. 7 K). Ryk-mCherry in response to Wnt5b stimulus presents with only 18 ± 2% Dvl-EGFP colocalization (Fig. 7, H–K) and internal Dvl-EGFP distribution instead of membrane (Fig. 7 I). We conclude that Wnt5b–Ryk and Wnt5b–Fz2 interactions demonstrate distinguishable effects on Dvl localization and cellular protrusions, suggesting that the two pathways lead to distinct downstream events.

Directional output from Wnt5b–Ryk interaction

Wnts are believed to have a permissive role in PCP through activating Fz receptors (Rohde and Heisenberg, 2007; Simons and Mlodzik, 2008). Yet Wnt5a functions as a directional cue in Ryk-mediated axon pathfinding (Yoshikawa et al., 2001; Liu et al., 2005; Keeble and Cooper, 2006; Keeble et al., 2006). To test whether Wnt5b–Ryk signaling provides directional cues for cell movement, we adapted an animal cap explant co-culture assay developed to monitor Eph/Ephrin-mediated repulsion in zebrafish (Mellitzer et al., 1999). We generated Wnt5b directional signals by juxtaposing a Wnt5b-IRES-EGFP-CAAX–injected cap with a Wnt5b MO–injected cap (Fig. 8 A). A control mCherry-CAAX–injected cap co-cultured with an EGFP-CAAX–injected cap showed intermingling of EGFP- and mCherry-expressing cells (Fig. 8, B and H). Similarly, a Wnt5b-expressing cap co-cultured with an Fz2-mCherry/Wnt5b MO–injected cap revealed intermingling of EGFP and mCherry cells (Fig. 8, C and H). In contrast, a Wnt5b-expressing cap co-cultured with an Ryk-mCherry/Wnt5b MO–injected cap did not show cell intermingling (Fig. 8, E and H); rather, a border of reduced Ryk-mCherry signals, approximately three to four cells wide, was found at the interface of the two caps (Fig. 8 E, asterisk). This gap was not caused by cell loss (Fig. S4, A and B) and indicates potential receptor turnover. Because *wnt11* mutants also demonstrate CE defects (Heisenberg et al., 2000), we evaluated Ryk response to a directional Wnt11 signal. A Wnt11-expressing cap co-cultured with a Ryk-mCherry–expressing cap showed intermingling of cells (Fig. 8, D and H). Collectively, these data reveal that Wnt5b- and Ryk-expressing cells do not intermingle and suggest that Ryk is turned over in the presence of sustained Wnt5b signals.

We noted that Ryk-mCherry–expressing cells at the interface showed the leading edge oriented away from the Wnt5b source (Fig. 8 F, arrowhead); therefore, we performed time-lapse imaging to follow cell movement, as well as the direction of lamellipodia-like protrusions. To follow membrane dynamics, EGFP-CAAX was co-injected with *ryk* RNA or Ryk MO in donor embryos. Cells from these donor embryos were transplanted into the center of the animal cap aggregate generated from a *wnt5b* RNA–injected cap juxtaposed with a Wnt5b MO–injected cap (Fig. 9 A). Transplanted cells were imaged over time to evaluate active extension and retraction of lamellipodia-like protrusions (Fig. 9 B). Lamellipodia-like protrusions from *ryk* RNA–injected cells demonstrated polarized projection, with 72% of the protrusions directed away from the Wnt5b source (Video 5); in contrast, protrusions from Ryk MO–injected cells were random, with 52% directed away from and 48% directed toward the Wnt5b source (Video 6). Compared with Ryk MO–injected cells (0.70 ± 0.01), *ryk* RNA–injected cells transplanted into the aggregate showed reduced roundness (0.57 ± 0.01) reflective of increased

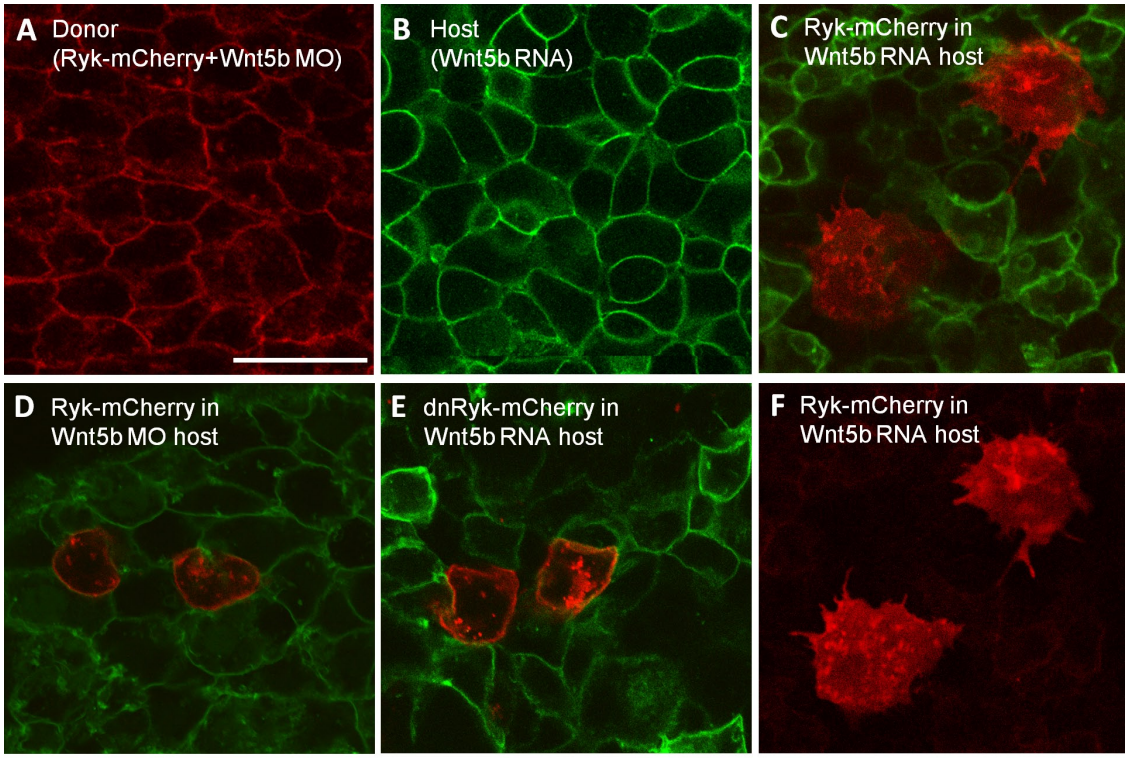

G

		Donor	Host
1	◆	dnRyk-mCherry + Wnt5b MO	Wnt5b-IRES-EGFP-CAAX
2	■	Ryk-mCherry + Wnt5b MO	EGFP-CAAX + Wnt5b MO
3	▲	mCherry-CAAX + Wnt5b MO	EGFP-CAAX + Wnt5b MO
4	×	Ryk-mCherrry + Wnt5b MO	Wnt5b-IRES-EGFP-CAAX

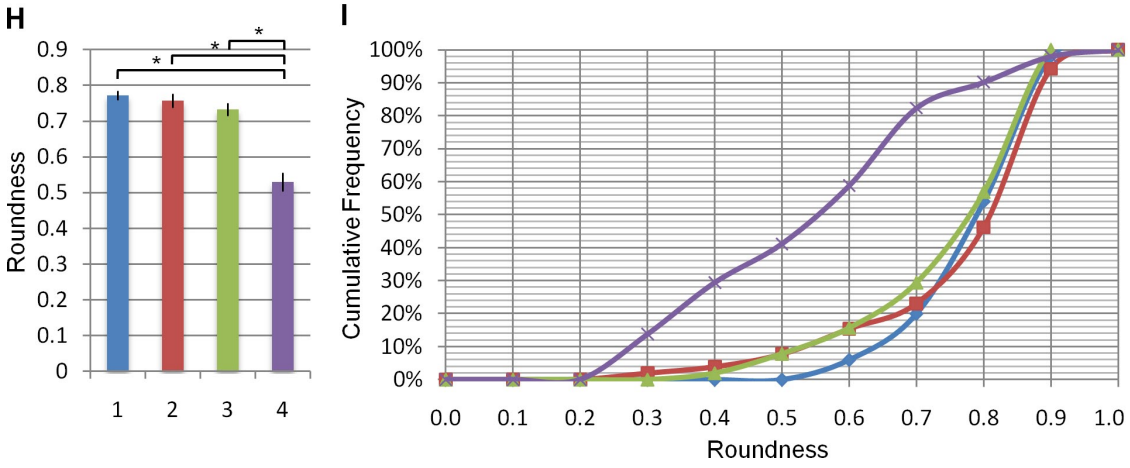

Figure 6. **Ryk-expressing cells respond to Wnt5b stimulus by internalizing Ryk and protrusion formation.** (A–F) Confocal images of hypoblast cells in 90% epiboly stage embryos, lateral view. (A and B) Donor embryo with Ryk-mCherry and Wnt5b MO (A); host embryo with Wnt5b-IRES-EGFP-CAAX (B). (C) Donor Ryk-mCherry + Wnt5b MO cells (red) transplanted into a Wnt5b-IRES-EGFP-CAAX host (green). (F) Red channel from C showing Ryk internalization and extensive protrusion formation in the transplanted cells. (D) Donor Ryk-mCherry + Wnt5b MO cells transplanted into an EGFP-CAAX + Wnt5b MO host. (E) Donor dnRyk-mCherry + Wnt5b MO cells transplanted into Wnt5b-IRES-EGFP-CAAX host (E). (G–I) Measurement of cell roundness frequency of transplanted cells. (G) Donor and host combination and the color code for each transplantation experiment (group 1–4) are listed. (H and I) A column chart shows the mean roundness and standard error (H), and a cumulative frequency chart shows the distribution of roundness for each group (I). 50 cells were measured for each group. One-way analysis of variance and Tukey's honestly significant difference test were applied, showing that group 4 is significantly different than groups 1–3 (*, $P < 0.01$). Bar, 30 µm.

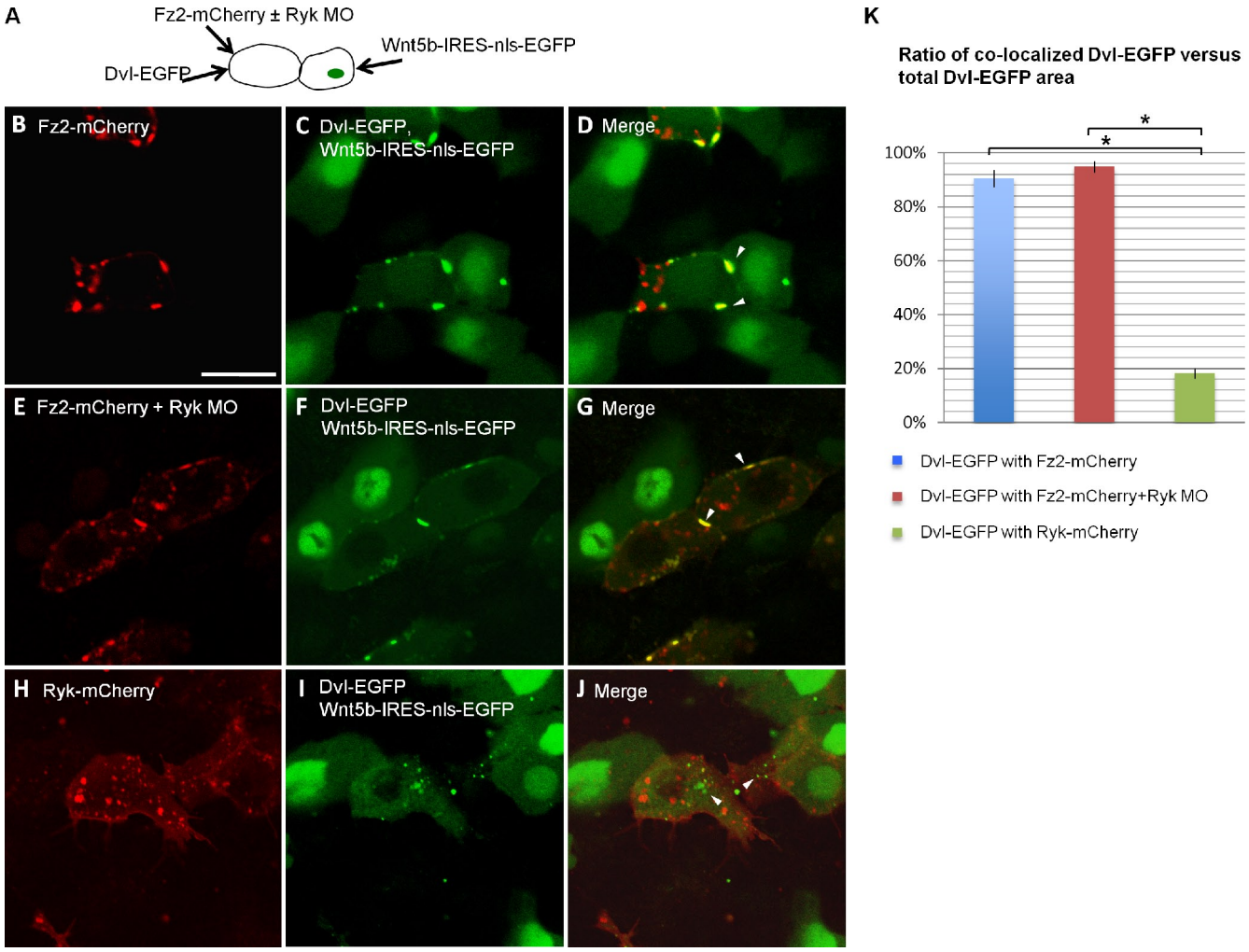

Figure 7. **Fz2 but not Ryk recruits Dvl.** (A) Schematic of mosaic injection approach. At the 8–16-cell stage, one cell was injected with Wnt5b-IRES-nls-EGFP RNA while an adjacent cell was injected with Dvl-EGFP RNA alone or combined with Fz2-mCherry RNA, Fz2-mCherry RNA + Ryk MO, or Ryk-mCherry RNA. (B–D) Fz-mCherry (B) when co-injected with Dvl-GFP (C) is concentrated in discrete membrane domains and colocalized with Dvl-EGFP (D, arrowheads) when adjacent to a Wnt5b-expressing cell (C and D; nuclear EGFP). (E–G) The pattern of Fz-mCherry (E) colocalized with Dvl-GFP (F and G) is not affected by co-injection of Ryk (G). Arrowheads in G mark the location of Dvl-EGFP. (H–J) Ryk-mCherry (H) when co-injected with Dvl-GFP (I) does not colocalize with Dvl-EGFP (J). Note that Ryk-expressing cells develop lamellipodia-like protrusions (H), and Dvl-EGFP is largely located in cytoplasmic areas that are Ryk-mCherry negative (J, arrowheads). (K) Quantification of the ratio of colocalized Dvl-EGFP versus total Dvl-EGFP area. Column height represents mean ratio in percentage. Error bars represent standard error of seven samples in each experiment. One-way analysis of variance and Tukey's honestly significant difference test were used (*, $P < 0.01$). Bar, 10 µm.

protrusions and cell elongation (Fig. 9 C). These results are consistent with transplantation experiments described in Fig. 6 and suggest that a Wnt5b can be translated into directional cue by Ryk-expressing cells.

Lateral mesoderm cells migrate at a total speed of ~70 µm/h (net dorsal speed at ~40 µm/h) in zebrafish embryos at 80–85% epiboly stage (von der Hardt et al., 2007). Tracking individual Ryk-expressing cells shows migration at a total speed of 105 ± 5 µm/h and net speed away from the Wnt5b source of 51 ± 7 µm/h (Fig. 9 D, Fig. S4 C, and Video 5). In contrast, Ryk MO–injected cells were relatively immobile (total speed at 40 ± 3 µm/h and net speed away from the Wnt5b source at 8 ± 4 µm/h; Fig. 9 D, Fig. S4 D, and Video 6). To monitor protrusive activity in epiboly stage embryos, Ryk-mCherry and Wnt5b-IRES-nls-EGFP RNAs were injected into individual cells to generate mosaic expression (Fig. 9 E). Ryk-mCherry cells adjacent to a Wnt5b-producing cell demonstrated distinct cell shape changes with lamellipodia-like protrusions projected away from the Wnt5b source (Fig. 9 F, arrowhead).

To determine whether Ryk activity was necessary for the directional projection of lamellipodia, Ryk MO was co-injected with mCherry-CAAX and, when adjacent to a Wnt5-producing cell, showed random projections relative to the Wnt5b source (Fig. 9 G, arrowhead). A majority of Ryk-expressing cells individually adjacent to one Wnt5b-expressing cell (77%; $n = 35$) showed protrusions opposite to the Wnt5b source, whereas only 17% of Ryk-deficient cells ($n = 36$) showed distinct protrusions opposite to the Wnt5b source. Collectively, these data suggest that Wnt5b–Ryk signaling polarizes cellular projections and directional cell migration.

Functional analysis of Ryk domains

To investigate the functional role of Ryk processing in zebrafish development, we generated a Flag-Ryk-myc construct (Fig. 10 A).

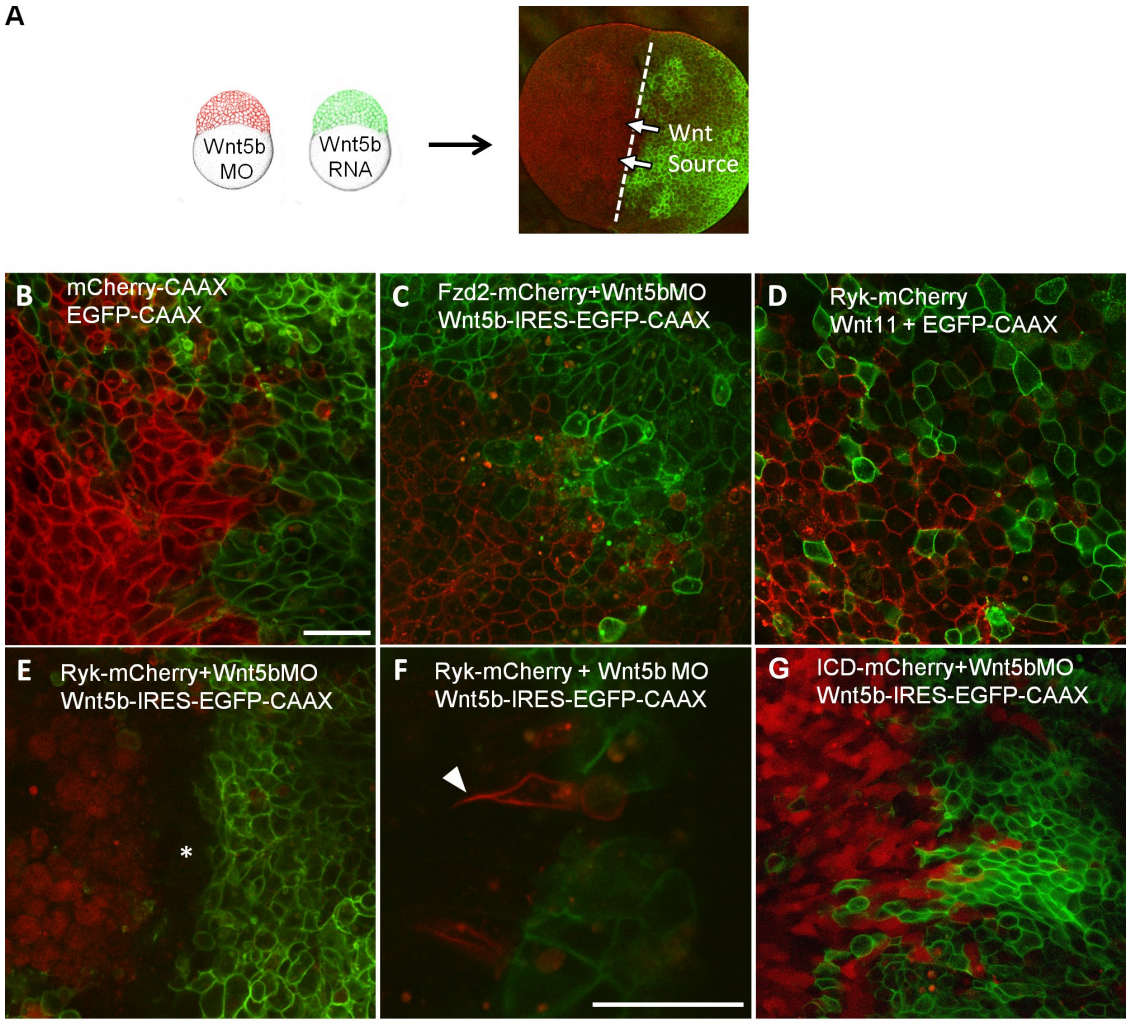

H

Red Moiety	Green Moiety	Non-intermingled	Intermingled
mCherry-CAAX+Wnt5bMO	Wnt5b-IRES-EGFP-CAAX	0	12
Fzd2-mCherry+Wnt5bMO	Wnt5b-IRES-EGFP-CAAX	1	16
Ryk-mCherry+Wnt5bMO	Wnt5b-IRES-EGFP-CAAX	17	2
Ryk-mCherry	Wnt11 + EGFP-CAAX	1	20
ICD-mCherry+Wnt5bMO	Wnt5b-IRES-EGFP-CAAX	0	15

Figure 8. **Zebrafish animal cap aggregate assays.** (A) The two co-cultured zebrafish animal caps were dissected from embryos injected with 100 pg Wnt5b-IRES-EGFP-CAAX (green) and 100 pg mCherry constructs + 1.0 pmol Wnt5b MO (red), respectively; a directional Wnt5b signal was created by juxtaposing the two caps. (B–G) Live images at the interface of co-cultured cap aggregates. (B) mCherry-CAAX cap (red) co-cultured with EGFP-CAAX cap (green) shows cell intermingling at the interface. (C) Fz2 (Fzd2)-mCherry + Wnt5b MO cap (red) co-cultured with Wnt5b-expressing cap (green) shows similar cell intermingling. (D) Wnt11-expressing cap (green) co-cultured with Ryk-mCherry–expressing cap (red) shows intermingled cells. (E) Ryk-mCherry + Wnt5b MO cap (red) co-cultured with Wnt5b-expressing cap (green) does not show intermingled cells. The region at the interface of the caps shows a distinct border with reduced Ryk-mCherry (asterisk). (F) High-magnification image of Ryk-mCherry–expressing cell projecting a protrusion away from the Wnt5b source. The arrowhead marks the leading edge of a Ryk-mCherry–expressing cell. (G) Ryk ICD-mCherry cap (red) co-cultured with Wnt5b-expressing cap (green) shows cell mixing. (H) Quantification of the number of cap aggregates that had cell intermingling at the interface. Bars, 20 µm.

First, we confirmed that Wnt5b reduces Ryk levels in a dose-dependent manner (Fig. 10 B), which is consistent with the cap aggregate results (Fig. 8 E). Most of the Ryk protein was found in a truncated form, with a size similar to the ICD of Ryk and suggestive that processing is important for Ryk function. In fact, a constitutive cleavage event within the ECD of Ryk was predicted (Halford and Stacker, 2001) and is consistent with our data. Additionally, the structurally related human WIF-1 protein is predicted to have disulfide bond formation between conserved cysteines (Liepinsh et al., 2006). The conserved C155 and C188 amino acids in the Ryk WIF domain would allow cleavage products to remain bound to each other (Fig. S5 B; Halford and Stacker, 2001); however, it remains unclear whether this binding occurs in vivo and its functional relevance. Therefore, we generated a point mutation in the conserved C155 (C155A) to disable disulfide bond formation. N-terminal Flag

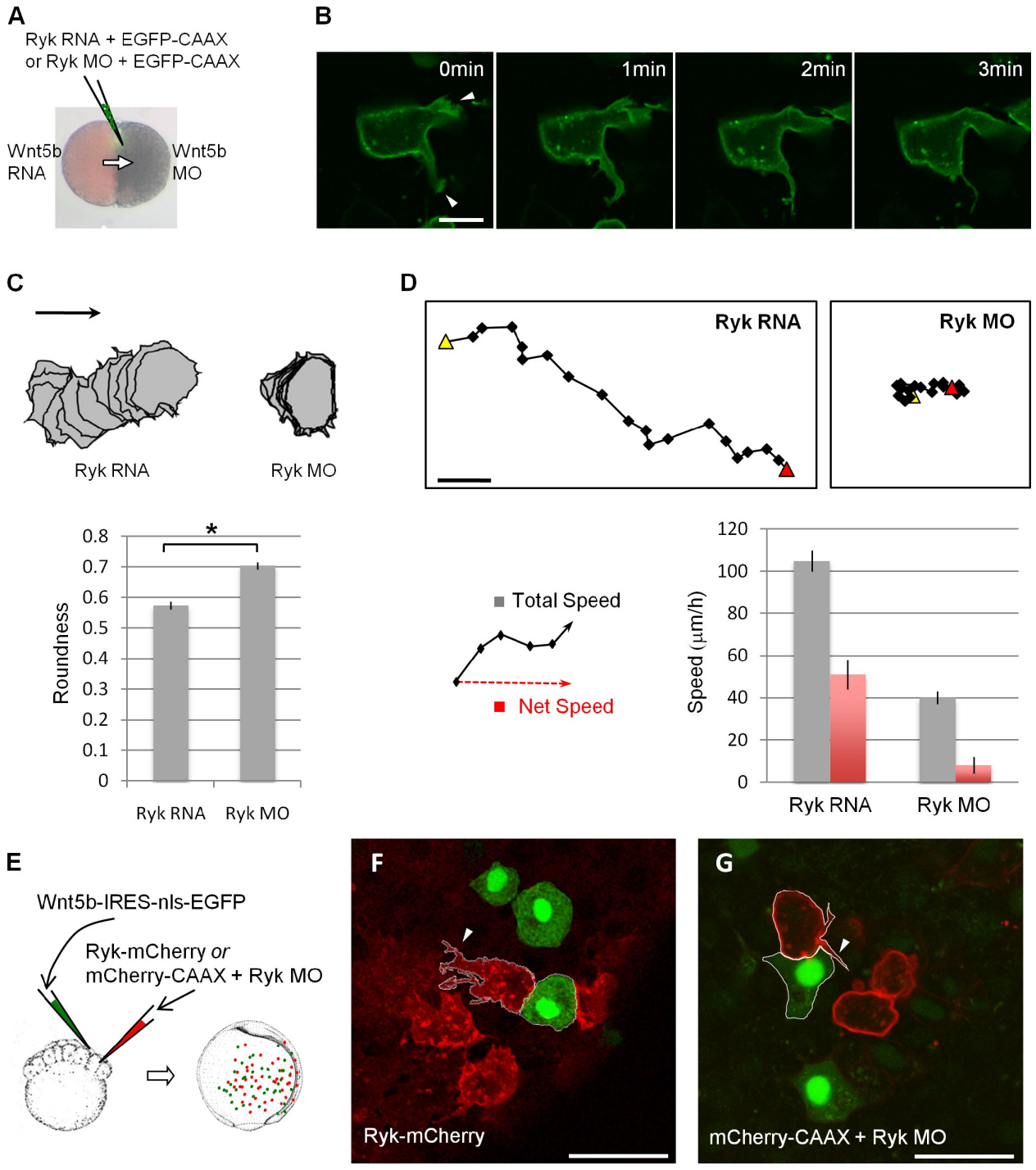

Figure 9. **Direction of Wnt5b–Ryk signaling is correlated with cell mobility and polarized cell protrusions.** (A) A *wnt5b* RNA–injected cap (red) and a Wnt5b MO–injected cap were juxtaposed and co-cultured to generate a directional Wnt source. Cells with *ryk* RNA + EGFP-CAAX or Ryk MO + EGFP-CAAX (green) were transplanted to the center of the aggregate interface. (B) An example of cell tracking of one *ryk* RNA–injected cell showing active extension and retraction of lamellipodia-like protrusions over time (arrowheads). (C) Overlay traces of a *ryk* RNA–injected cell (Video 5) and a Ryk MO–injected cell (Video 6); the arrow marks the direction of Wnt5b gradient (high to low) that was used to calculate cell roundness and was significantly different between *ryk* RNA– and Ryk MO–injected cells. Error bars represent standard error ($n = 24$; Student's *t* test: *, $P < 0.01$). (D) Representative migration path of individual cells recorded by time-lapse imaging over 20 min at 1-min intervals; start and end points are indicated by yellow and red triangles, respectively; Wnt5b source to the left. Total speed in all directions (black curved arrow) and net speed away from the Wnt5b source (red dashed arrow) are charted comparing Ryk MO–injected cells with Ryk RNA–injected cells ($n = 10$). Error bars represent standard error. (E–G) Polarized lamellipodia-like protrusions in 80–90% epiboly stage embryos. (E) Schematic of the mosaic injection experimental approach. (F) Ryk-mCherry cells (red) adjacent to Wnt5b-IRES-nls-EGFP cells (green) show directional protrusions (arrowhead). (G) mCherry-CAAX and Ryk MO cell (red) adjacent to Wnt5b-IRES-nls-EGFP cells (green) display random projections (arrowhead). (F and G) White lines outline a Wnt5b-expressing cell (green) and an adjacent cell injected with mCherry constructs (red). Bars: (B) 10 μm; (D) 5 μm; (F and G) 30 μm.

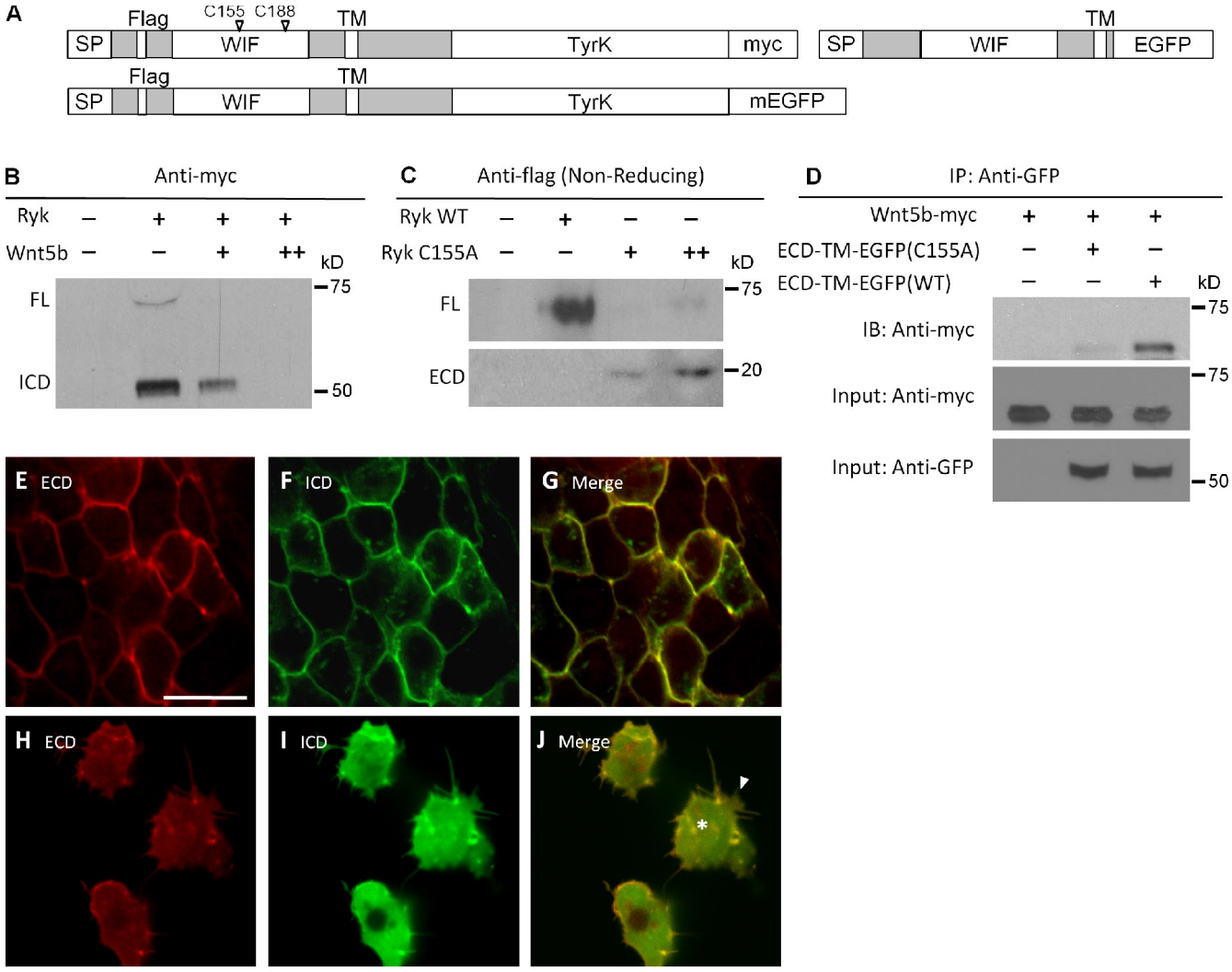

Figure 10. **Ryk processing and domain localization.** (A) Schematic of three different Ryk expression constructs. The positions of C155 and C188 are noted. SP, signal peptide; WIF, Wnt-inhibitory factor domain; TM, TM domain; TyrK, tyrosine kinase domain. (B) Western blot analysis of Flag-Ryk-myc with increasing amounts of Wnt5b reveals Ryk cleavage with ICD and turnover. Tagged Ryk RNA was injected at 20 pg; Wnt5b RNA was injected at 5 (+) and 10 pg (++). (C) Western blot analysis of Flag-Ryk-myc under nonreducing conditions showing differential accumulation of Ryk full-length (FL) and ECD forms with wild-type (WT) and Ryk C155A ECD expression constructs. *ryk* RNA was injected at 20 pg; *ryk* C155A RNA was injected at 20 (+) and 50 pg (++). (D) Coimmunoprecipitation analysis showing that Wnt5b-myc interacts with Ryk ECD-TM-EGFP and not with Ryk C155A mutant. Wnt5b-myc was injected at 10 pg; wild-type and C155A ECD-TM-EGFP were injected at 50 pg. IB, immunoblot; IP, immunoprecipitation. (E–G) In donor embryos, Flag tag detects ECD (E), and C-terminal monomeric EGFP detects ICD (F) at 80–90% epiboly; merged images are shown (G). (H–J) After transplantation into a Wnt5b-expressing host, both ECD (H) and the ICD (I) show internalization; merged images are shown in J and coarse colocalization (asterisk). Note increased protrusive activity of the transplanted cell (J, arrowhead). Bar, 20 µm.

tag allows identification of full-length size Ryk or processed ECD based on size. Under nonreducing conditions to maintain the disulfide bond, full-length size Ryk was observed with no detectable ECD product (Fig. 10 C). Conversely, expression of the Ryk-C155A point mutation resulted in accumulation of Ryk ECD (Fig. 10 C), indicating that there is a cleavage site in the ECD and that a disulfide bond formed between Ryk products requires C155.

To determine whether Wnt5b–Ryk interaction depends on the disulfide bond formation, we performed coimmunoprecipitation using myc-tagged Wnt5b and EGFP-tagged Ryk constructs (Fig. 10 A). Because Wnt5b induces significant turnover of Ryk (Fig. 10 B) and both the ECD and full-length Ryk can bind to Wnt5a (Yoshikawa et al., 2003; Liu et al., 2005; Keeble et al., 2006; Kim et al., 2008), we generated an ECD-TM-EGFP construct for coimmunoprecipitation (Fig. 10 A). Anti-GFP antibody precipitated Wnt5b-myc when it was coexpressed with ECD-TM-EGFP; however, little Wnt5b-myc was coimmunoprecipitated with the ECD-TM-EGFP point mutant (C155A; Fig. 10 D). Thus, we demonstrate that the cleaved ECD is bound to the remaining Ryk product and that this structural feature is critical for Wnt5b binding.

Similar to mammalian Ryk protein (Lyu et al., 2008), zebrafish Ryk is cleaved by γ-secretase at the TM, and this Ryk processing is sensitive to γ-secretase inhibitor DAPT (Fig. S5 A). Because most of the expressed Flag-Ryk-myc protein was found in the ICD size by anti-myc (Fig. 10 B), and the mammal processed ICD was shown to drive neuronal differentiation in cell culture (Lyu et al., 2008), we performed functional assays with Ryk ICD. We have shown that although

full-length Ryk–expressing cells do not mix with Wnt5b-IRES-EGFP-CAAX–injected cells in animal cap aggregates (Fig. 8, E and H), Ryk ICD-mCherry–expressing cells intermingled with Wnt5b-expressing cells (Fig. 8, G and H). Moreover, Ryk ICD was not sufficient to suppress Ryk MO–induced CE defects (Fig. 2 G). These data suggest that Ryk ICD alone is not sufficient to substitute for full-length Ryk. To evaluate ECD and ICD distribution in response to Wnt5b, we performed cell transplantation assays. In donor embryos expressing Flag-Ryk-EGFP, both ECD (Flag; Fig. 10 E) and ICD (EGFP; Fig. 10 F) show membrane localization (Fig. 10 G). When transplanted into a Wnt5b-expressing host, the Flag-Ryk-EGFP–expressing cells show increased protrusive activities (Fig. 10 J, arrowhead), and both the ECD and ICD are internalized with overlapping localization (Fig. 10 J, asterisk). These data coupled with the functional analyses suggest that cell shape changes in response to Wnt5b do not require the separation of Ryk ECD and ICD, and in fact, both portions of Ryk are required to properly convey directional Wnt5b signals.

Discussion

Wnt signaling, through RTK receptors such as Ror2, has been shown to provide alternative mechanisms for proper CE movements (Schambony and Wedlich, 2007). Ryk knockdown in *Xenopus* results in gastrulation defects (Kim et al., 2008), and surviving Ryk knockout mice display truncated bodies, craniofacial defects, and significantly shortened limbs (Halford et al., 2000). A human *RYK* mutation is associated with a nonsyndromic cleft lip and palate, indicative of migration defects (Watanabe et al., 2006). In this study, we show that Ryk function is necessary to convey Wnt5b signals for directional cell movement during zebrafish gastrulation.

Although, zebrafish Wnt5a (Stoick-Cooper et al., 2007) is expressed at low levels during gastrulation, knockdown did not result in CE defects (unpublished data); however, this does not exclude a role for Wnt5a–Ryk at other stages. Both *ryk* and *wnt5b* transcripts are found in the developing eye, and we identified similar IPL defects in the retinas of both Ryk and Wnt5b knockdown embryos in addition to shared CE defects (Fig. 2). Other Wnts are likely involved with Ryk in patterning neuronal projections, specifically Wnt3a, which is expressed in the zebrafish brain (Krauss et al., 1992) and has been shown to be Ryk dependent in murine axon pathfinding (Schmitt et al., 2006) and neurite outgrowth in dorsal root ganglia explants (Lu et al., 2004). Overlapping defects in Ryk and Wnt5b knockdown (Fig. 2), with the synergistic interaction of subphenotypic MO combinations (Fig. 3), support the idea that Wnt5b is the predominant ligand for Ryk during gastrulation.

Zygotic *wnt5b/pipetail* mutants show reduced Ca^{2+} release (Westfall et al., 2003a), whereas overexpression of Wnt5b activates Ca^{2+} release (Fig. 4 E). We determined that Ryk is necessary for Wnt5b-induced Ca^{2+} release activity (Fig. 4). Notably, Ryk knockdown did not completely suppress Wnt5-induced activity, suggesting that Wnt5b-induced Ca^{2+} release requires other components. This finding is consistent with both our demonstration of Fz mediating Wnt/Ca^{2+} signaling in zebrafish embryos (Slusarski et al., 1997a; Liu et al., 1999; Ahumada et al., 2002) and the finding that application of Wnt5a to neurons evokes intracellular Ca^{2+} release through both Ryk and Fz receptors (Li et al., 2009). Therefore, Ryk is necessary but not the sole receptor for Wnt5b-induced Ca^{2+} release.

Combinations of specific Wnt receptors have been shown to influence distinct downstream signaling events (van Amerongen et al., 2008). Indeed, in *C. elegans* development, a combination of Fz, Ryk, and the Ror RTK CAM-1 signaling leads to proper orientation of vulval cells (Green et al., 2008). Our data indicate that Wnt5b–Ryk and Wnt5b–Fz2 pathways lead to distinct signaling outputs. In the presence of Wnt5b, Fz2 but not Ryk clusters with Dvl on the membrane (Fig. 7). This, along with the intermingling of Fz and Wnt5b but not Ryk and Wnt5b cells in co-cultured animal caps (Fig. 8), is consistent with our hypothesis that Ryk and Fz2 pathways are separate. We postulate that Wnt5b–Fz2 activates a PCP-like pathway similar to Wnt11–Fz7 signaling that is directly associated with Dvl (Witzel et al., 2006; Carmona-Fontaine et al., 2008). In contrast to a previous study in *Xenopus* (Kim et al., 2008), we demonstrate that Wnt5b is largely responsible for Ryk-mediated gastrulation movement by promoting Ryk internalization and efficient persistent cell protrusions with net migration away from the Wnt5b source (Figs. 6, 8, and 9). Although the possibility of compound signaling from Fz/Ryk coreceptor remains, given the distinct individual responses to Wnt5b, it is likely that this would lead to different downstream events than either receptor alone.

Furthermore, we demonstrate that Ryk ECD processing is necessary for Ryk and Wnt5b binding. Although the ICD portion of Ryk is sufficient to drive neuronal differentiation in cell culture (Lyu et al., 2008), our work demonstrates that Ryk ICD–expressing cells intermingle with Wnt5b-expressing cells in co-cultured animal caps, and expression of ICD alone does not rescue Ryk MO–induced CE defects in zebrafish (Fig. 8). We postulate that lack of rescue suggests Wnt5b and Ryk ECD interaction is necessary for directional cell migration and that nondirectional Ryk signaling is insufficient to mediate CE movement. Moreover, our results show both ECD and ICD portions of Ryk are internalized upon Wnt5b exposure (Fig. 10), indicating that Wnt5b-mediated protrusive activities require full-length Ryk. These observations differ from nondirectional responses like neuronal differentiation that require accumulation of ICD in the nucleus (Lyu et al., 2008).

Noncanonical Wnts are speculated to function as permissive cues that do not provide positional signals to components of the PCP pathway (Rohde and Heisenberg, 2007; Simons and Mlodzik, 2008). Unlike the *wnt11/silberblick* mutant (Heisenberg et al., 2000), the phenotype of *wnt5b/pipetail* cannot be rescued by *wnt5b* RNA expression (Kilian et al., 2003; Westfall et al., 2003a), suggesting that localized Wnt5b can provide essential spatial information. Consist with providing spatial cues, zygotic *wnt5b* expression is localized in the ventral–posterior region (Kilian et al., 2003), with a graded expression pattern resembling that of mammalian Wnt5a (Yamaguchi et al., 1999). We tested the hypothesis that a Wnt5b gradient could be conveyed to Ryk-expressing cells by co-culturing assays. We found that Wnt5b–Ryk interaction restricted cells intermingling, whereas Wnt11–Ryk

cells freely intermingled (Fig. 8). Moreover, lamellipodia-like protrusions of Ryk-expressing cells are projected away from the Wnt5b source, which may underlie repulsive migration (Fig. 9). However, other mechanisms such as changes in cell adhesion and/or cortical tension that could have a role in Ryk-regulated cell motility were not addressed in this study. Based on these observations, we predict that Wnt5b–Ryk in addition to Wnt5b–Fz interactions contribute to the *wnt5b/pipetail* mutant phenotype. Our data support a model in which Wnt5b can act as both a permissive cue through Fz and core PCP components and as an instructive cue through Ryk to regulate directional cell migration during gastrulation.

Materials and methods

Zebrafish embryo maintenance and staging
Zebrafish embryos were collected from natural spawning. Staging was performed according to Kimmel et al. (1995). Live embryos were photographed after orienting in 3% methylcellulose.

Morpholinos, expression constructs, and PCR primers
MOs were obtained from Gene Tools, LLC and are as follows: control, 5′-CCTCTTACCTCAGTTACAATTTATA-3′; Wnt5b MO, 5′-GCAAACACAATAATTTCTTACCACC-3′; Ryk MO1, 5′-GGCGACATGCTACTGGGTTTTGACG-3′; and Ryk MO2, 5′-ATCGACCAGCGCCACGGAACCTCAT-3′. Dvl-EGFP and Wnt11 expression constructs were obtained from D. Houston (University of Iowa, Iowa City, IA) and M. Furutani-Seiki (University of Bath, Bath, England, UK), respectively. Zebrafish *ryk* (Ensembl Zv8 gene identifier ENSDARG00000007231), *wnt5b,* and *fz2* were cloned from a mixture of cDNAs for 0–24-hpf zebrafish embryos with GeneAmp high-fidelity polymerase (Applied Biosystems). The following primer pairs were used for PCR reactions: Wnt5b, 5′-CTGCTGTTTTGAGGGGATTC-3′ and 5′-CGCACTGAGCAATTAAGCAG-3′; full-length Ryk with the stop codon, 5′-ACTTTTTAAAGCGACGGTGG-3′ and 5′-ATCAACAACTCGGCTGGTTT-3′; full-length Ryk without the stop codon, 5′-TAAAGCGACGGTGGGCTGTG-3′ and 5′-CACGTAGGCCCCCAAAGCTG-3′; dnRyk, 5′-GGTGGGCTGTGATGTTTCTG-3′ and 5′-CCTCTTCATGCTGTGGAGGT-3′; 5′ UTR of the *ryk* gene, 5′-GAGCGCGAGCTAACAGAAGT-3′ and 5′-GAGCAGCAGGAGGAGAAAGA-3′; Ryk ICD, 5′-GTGGAAATGGATGACAGCGT-3′ and 5′-CACGTAGGCCCCCAAAGCTG-3′; and Fz2, 5′-GTTTGCCGGACTCATTTTGTA-3′ and 5′-AACAGTGGTTTCTCCTTGTCC-3′. PCR products were cloned into pCR8/GW/TOPO entry vector and integrated into destination clones by LR Clonase enzyme mix (Invitrogen). 3′ entry clones and destination vectors were from N. Lawson's laboratory (University of Massachusetts Medical School, Worcester, MA) and from the Tol2kit (C. Chien, University of Utah, Salt Lake City, UT; Kwan et al., 2007). Synthetic RNAs were made with mMessage mMachine Capped RNA transcription kit (Applied Biosystems). Semiquantitative RT-PCR used 5′-CTGGTCCACATGGCAATACA-3′ and 5′-CTGGTTTGGGCCAGTTTACA-3′ for *ryk* and 5′-TCAGCCATGGATGATGAAAT-3′ and 5′-GGTCAGGATCTTCATGAGGT-3′ for β-actin, with Advantage 2 polymerase (Takara Bio Inc.) in 30 cycles with the annealing step lasting 2 min at 57°C.

Injection and transplantation
Zebrafish embryos were injected at the one-cell stage into the yolk for global expression and at 16–32-cell stages into individual blastomeres for mosaic expression. For assessing cell migration by transplantation, a group of donor embryos was microinjected with Ryk MO mixed with 20 ng of lineage marker (dextran-conjugated Texas red; Invitrogen) at the one-cell stage. A second group of donor embryos was injected with FITC-conjugated control MO. A group of host embryos was injected with Wnt5 MO at the one-cell stage. Donor and host embryos were manually dechorionated before transplantation. Using a single needle, 10–20 cells were removed from each donor embryo at high-sphere stage, mixed, and transplanted into the center of lateral mesoderm of a host embryo at shield stage. Embryos with grafted cells were allowed to grow to tailbud stage for imaging. For assessing ligand-receptor interaction by transplantation, donor and host embryos were injected with 100 pg RNA. At sphere stage, ∼20 cells were transplanted into the blastodermal margin of each host embryo. At shield stage, embryos with transplanted cells at lateral or ventral mesoderm were selected and allowed to grow to 90–100% epiboly for imaging.

Whole-mount in situ hybridization and antibody staining
Hybridization and antibody staining was performed as described previously (Westfall et al., 2003b) with anti-myc antibody (9E10; Santa Cruz Biotechnology, Inc.) in 1:1500 dilution or rabbit anti-Flag (Sigma-Aldrich) in 1:200 dilution, followed by fluorescent secondary antibodies (Alexa Fluor 488, 568, or 633; Invitrogen).

Retina histology
The transgenic line *huc*:GFP [Tg (elav3:eGFP)] (Park et al., 2000) was evaluated at 3 dpf. MO-injected embryos were processed for cryosectioning as previously described (Baye and Link, 2007). In brief, embryos were infiltrated at 4°C in 15% sucrose, 30% sucrose, and overnight in 100% OCT (optimal cutting temperature) and then oriented in freezing molds and sectioned at −25°C. 12-µm cryosections were mounted on glass slides and coverslipped with Vectashield mounting media (Vector Laboratories) for confocal imaging.

Zebrafish animal cap aggregates
Experiments were performed as described previously (Mellitzer et al., 1999), with the exception that the aggregates were imaged alive in glass coverslips without fixation. In brief, embryos were injected at one-cell stages with 100 pg RNAs. At the 1,000-cell stage, embryos were dechorionated, and animal caps were dissected in L15 medium with 10% fetal calf serum. Animal caps were juxtaposed and healed for 10 min. Aggregate was mounted under a coverslip and cultured overnight. Fluorescent tracers were visualized with confocal microscopy. Nonintermingled aggregates showed a clear boundary (of the EGFP moiety) and a dark gap (from the mCherry moiety) wider than 30 µm in five nonoverlapping 5.7×10^{-8} m^2 squares at the interface. Intermingled aggregates showed skewed boundaries, uniform mCherry intensity, and at least five isolated mCherry-positive cell clusters per square in five nonoverlapping 5.7×10^{-8} m^2 squares at the interface.

For cell transplantation in the aggregates, animal caps were allowed to heal for 30 min in culture medium after juxtaposition. Cells from sphere/dome-stage donor embryos were transplanted to the center of the aggregates with a needle. The aggregates were healed in culture medium for 1 h and then mounted under a coverslip and cultured for an additional 1 h before imaging.

Image acquisition and analysis
Confocal images were acquired with a confocal microscope system (TCS SP2; Leica), using either a 63× NA 1.40 oil objective or a 20× NA 0.70 air objective on a heating stage at 30°C. Fixed samples were mounted in Vectashield mounting medium. Live samples were mounted in corresponding culture medium using bridged coverslips. Cell roundness was measured by ImageJ software (National Institutes of Health), which outlines cell perimeter including lamellipodia and lobopodia-like protrusions, and was defined as $4\pi A/P^2$ (possible roundness values are between 0 and 1), in which P is the perimeter of a cell and A is the area the cell occupied after the cytoplasmic region within the perimeter is filled with corresponding color. Dvl-EGFP–, Fz2-mCherry–, or Ryk-mCherry–positive domains were measured by the ImageJ software with the "Colocalization" plugin.

Ca^{2+} activity images were acquired by an inverted epifluorescence microscope (Axiovert 100; Carl Zeiss, Inc.) with coverslip-bottomed heating chamber at 30°C, filters for epifluorescence (Chroma Technology Corp.), dual filter wheel, and 10× NA 0.50 Plan-Neofluar objective. A slow-scan charge-coupled device camera at high spatial resolution and high bit depth (12-bit grayscale; Quantix; Photometrics) was used. Data were collected at 15-s intervals as image pairs at 340- and 380-nm excitation wavelengths. Ratio images were calculated by the Ratio Tool software (Inovision). Texas red distribution was determined by collecting a reference exposure at 540-nm excitation. The high-resolution images used for the subtractive algorithm were converted to 8-bit images and exported into QuickTime (Apple) for generation of the supplemental videos.

Bright/darkfield and in situ hybridization images were acquired by a microscope (Stereo Discovery.V12; Carl Zeiss, Inc.) with AxioVision software (Carl Zeiss, Inc.) and X-Cite 120 light system (EXFO Photonic Solution Inc.), using either an Achromat S 1.0× NA 0.50 objective or a 10× NA 0.45 air objective at 30°C. Fixed sample was mounted in 1× PBS. Live sample was mounted in corresponding culture medium. CE index was defined as length to width ratio of the *myoD* domain (Angers et al., 2006). The length was defined as the distance between the anterior edge of the most rostral somite and the posterior edge of the most caudal somite. The width was defined as the distance between the left and right edges of the widest pair of somites. At the 10–11-somite stage, the mean CE index for wild-type embryos is 2.8; at the 13–14-somite stage, the mean CE index

for wild-type embryos is 3.5. Mean difference between distance travelled by Texas red and FITC cells was analyzed by ImageJ software. For individual embryos, the mean distance between green and red tracers was determined by $\Delta R = \bar{R}_{green} - \bar{R}_{red}$, in which $\bar{R}_{green}$ and $\bar{R}_{red}$ are the mean distance travelled by all green and red cells from the center of the embryos, respectively. ΔR from 10 embryos in the same experimental group was used to calculate the mean $\overline{\Delta R}$ and standard deviation within each group.

Western blot and coimmunoprecipitation

Injected embryos at 90% epiboly were lysed for analysis with mouse anti-myc antibody (9E10; Santa Cruz Biotechnology, Inc.) in 1:2,000 dilution, anti-GFP antibody (Roche) in 1:1,000 dilution, or mouse anti-Flag antibody (M2; Sigma-Aldrich) in 1:1,000 dilution. Anti–β-actin antibodies (Sigma-Aldrich) in 1:2,000 dilution were used for loading controls. Antioxidant reagents were omitted for nonreducing condition.

EGFP-tagged proteins were immunoprecipitated with anti-GFP antibody (Roche) in 1:100 dilution and protein A/G agarose (Thermo Fisher Scientific). The immunoprecipitates were washed four times at 4°C with buffer (50 mM Tris at pH 7.5, 150 mM NaCl, 0.8% Triton X-100, 0.5 mM PMSF, and leupeptin at 5 µg/ml).

Online supplemental material

Fig. S1 shows synteny of genomic regions of zebrafish *ryk* and human *RYK* and protein sequence alignment. Fig. S2 shows 5′ UTR–EGFP RNAs used to evaluate Ryk MO efficacy, Ryk MO phenotypes, and *ryk* RNA overexpression. Fig. S3 shows Ryk-mCherry localization, Fz2-mCherry + Wnt5b MO donor cells transplanted into a Wnt5b-expressing host, and Caveolin1-EGFP colocalization with Ryk-mCherry. Fig. S4 shows animal cap aggregates with nuclear EGFP and representative aggregates of *ryk* RNA– and Ryk MO–injected cells transplanted into animal caps. Fig. S5 shows Western blotting of DAPT-treated myc-tagged Ryk protein, the position of C155 and C188 in Ryk ECD, and a Ryk processing model. Videos 1–3 show the Ca^{2+} activity in a wild-type embryo, an embryo unilaterally injected with Ryk MO, and a *wnt5b* RNA–injected embryo, respectively. Video 4 shows the Ca^{2+} activity in an embryo globally injected with *wnt5b* RNA and unilaterally injected with Ryk MO. Videos 5 and 6 show the movement and cell shape changes of *ryk* RNA– and Ryk MO–injected cells, respectively, transplanted into an animal cap aggregate. Online supplemental material is available at http://www.jcb.org/cgi/content/full/jcb.200912128/DC1.

We thank Drs. D. Houston, C. Chien, N. Lawson, and M. Furutani-Seiki for reagents. We thank Drs. D. Houston and C. Stipp for comments on the manuscript.

This work was supported by National Institutes of Health grant CA112369 (to D.C. Slusarski).

Submitted: 18 December 2009
Accepted: 29 June 2010

References

Ahumada, A., D.C. Slusarski, X. Liu, R.T. Moon, C.C. Malbon, and H.Y. Wang. 2002. Signaling of rat Frizzled-2 through phosphodiesterase and cyclic GMP. *Science*. 298:2006–2010. doi:10.1126/science.1073776

Angers, S., C.J. Thorpe, T.L. Biechele, S.J. Goldenberg, N. Zheng, M.J. MacCoss, and R.T. Moon. 2006. The KLHL12-Cullin-3 ubiquitin ligase negatively regulates the Wnt-beta-catenin pathway by targeting Dishevelled for degradation. *Nat. Cell Biol.* 8:348–357. doi:10.1038/ncb1381

Baye, L.M., and B.A. Link. 2007. The disarrayed mutation results in cell cycle and neurogenesis defects during retinal development in zebrafish. *BMC Dev. Biol.* 7:28. doi:10.1186/1471-213X-7-28

Cadigan, K.M., and Y.I. Liu. 2006. Wnt signaling: complexity at the surface. *J. Cell Sci.* 119:395–402. doi:10.1242/jcs.02826

Carmona-Fontaine, C., H.K. Matthews, S. Kuriyama, M. Moreno, G.A. Dunn, M. Parsons, C.D. Stern, and R. Mayor. 2008. Contact inhibition of locomotion in vivo controls neural crest directional migration. *Nature*. 456:957–961. doi:10.1038/nature07441

Freisinger, C.M., I. Schneider, T.A. Westfall, and D.C. Slusarski. 2008. Calcium dynamics integrated into signalling pathways that influence vertebrate axial patterning. *Philos. Trans. R. Soc. Lond. B Biol. Sci.* 363:1377–1385. doi:10.1098/rstb.2007.2255

Green, J.L., T. Inoue, and P.W. Sternberg. 2008. Opposing Wnt pathways orient cell polarity during organogenesis. *Cell*. 134:646–656. doi:10.1016/j.cell.2008.06.026

Halford, M.M., and S.A. Stacker. 2001. Revelations of the RYK receptor. *Bioessays*. 23:34–45. doi:10.1002/1521-1878(200101)23:1<34::AID-BIES1005>3.0.CO;2-D

Halford, M.M., J. Armes, M. Buchert, V. Meskenaite, D. Grail, M.L. Hibbs, A.F. Wilks, P.G. Farlie, D.F. Newgreen, C.M. Hovens, and S.A. Stacker. 2000. Ryk-deficient mice exhibit craniofacial defects associated with perturbed Eph receptor crosstalk. *Nat. Genet.* 25:414–418. doi:10.1038/78099

Harris, K.E., and S.K. Beckendorf. 2007. Different Wnt signals act through the Frizzled and RYK receptors during *Drosophila* salivary gland migration. *Development*. 134:2017–2025. doi:10.1242/dev.001164

Heisenberg, C.P., M. Tada, G.J. Rauch, L. Saúde, M.L. Concha, R. Geisler, D.L. Stemple, J.C. Smith, and S.W. Wilson. 2000. Silberblick/Wnt11 mediates convergent extension movements during zebrafish gastrulation. *Nature*. 405:76–81. doi:10.1038/35011068

Inoue, T., H.S. Oz, D. Wiland, S. Gharib, R. Deshpande, R.J. Hill, W.S. Katz, and P.W. Sternberg. 2004. *C. elegans* LIN-18 is a Ryk ortholog and functions in parallel to LIN-17/Frizzled in Wnt signaling. *Cell*. 118:795–806. doi:10.1016/j.cell.2004.09.001

Keeble, T.R., and H.M. Cooper. 2006. Ryk: a novel Wnt receptor regulating axon pathfinding. *Int. J. Biochem. Cell Biol.* 38:2011–2017. doi:10.1016/j.biocel.2006.07.005

Keeble, T.R., M.M. Halford, C. Seaman, N. Kee, M. Macheda, R.B. Anderson, S.A. Stacker, and H.M. Cooper. 2006. The Wnt receptor Ryk is required for Wnt5a-mediated axon guidance on the contralateral side of the corpus callosum. *J. Neurosci.* 26:5840–5848. doi:10.1523/JNEUROSCI.1175-06.2006

Kilian, B., H. Mansukoski, F.C. Barbosa, F. Ulrich, M. Tada, and C.P. Heisenberg. 2003. The role of Ppt/Wnt5 in regulating cell shape and movement during zebrafish gastrulation. *Mech. Dev.* 120:467–476. doi:10.1016/S0925-4773(03)00004-2

Kim, G.H., J.H. Her, and J.K. Han. 2008. Ryk cooperates with Frizzled 7 to promote Wnt11-mediated endocytosis and is essential for *Xenopus laevis* convergent extension movements. *J. Cell Biol.* 182:1073–1082. doi:10.1083/jcb.200710188

Kimmel, C.B., W.W. Ballard, S.R. Kimmel, B. Ullmann, and T.F. Schilling. 1995. Stages of embryonic development of the zebrafish. *Dev. Dyn.* 203:253–310.

Krauss, S., V. Korzh, A. Fjose, and T. Johansen. 1992. Expression of four zebrafish wnt-related genes during embryogenesis. *Development*. 116:249–259.

Kwan, K.M., E. Fujimoto, C. Grabher, B.D. Mangum, M.E. Hardy, D.S. Campbell, J.M. Parant, H.J. Yost, J.P. Kanki, and C.B. Chien. 2007. The Tol2kit: a multisite gateway-based construction kit for Tol2 transposon transgenesis constructs. *Dev. Dyn.* 236:3088–3099. doi:10.1002/dvdy.21343

Li, L., B.I. Hutchins, and K. Kalil. 2009. Wnt5a induces simultaneous cortical axon outgrowth and repulsive axon guidance through distinct signaling mechanisms. *J. Neurosci.* 29:5873–5883. doi:10.1523/JNEUROSCI.0183-09.2009

Liepinsh, E., L. Bányai, L. Patthy, and G. Otting. 2006. NMR structure of the WIF domain of the human Wnt-inhibitory factor-1. *J. Mol. Biol.* 357:942–950. doi:10.1016/j.jmb.2006.01.047

Liu, X., T. Liu, D.C. Slusarski, J. Yang-Snyder, C.C. Malbon, R.T. Moon, and H. Wang. 1999. Activation of a frizzled-2/beta-adrenergic receptor chimera promotes Wnt signaling and differentiation of mouse F9 teratocarcinoma cells via Galphao and Galphat. *Proc. Natl. Acad. Sci. USA*. 96:14383–14388. doi:10.1073/pnas.96.25.14383

Liu, Y., J. Shi, C.C. Lu, Z.B. Wang, A.I. Lyuksyutova, X.J. Song, X. Song, and Y. Zou. 2005. Ryk-mediated Wnt repulsion regulates posterior-directed growth of corticospinal tract. *Nat. Neurosci.* 8:1151–1159. doi:10.1038/nn1520

Lu, W., V. Yamamoto, B. Ortega, and D. Baltimore. 2004. Mammalian Ryk is a Wnt coreceptor required for stimulation of neurite outgrowth. *Cell*. 119:97–108. doi:10.1016/j.cell.2004.09.019

Lyu, J., V. Yamamoto, and W. Lu. 2008. Cleavage of the Wnt receptor Ryk regulates neuronal differentiation during cortical neurogenesis. *Dev. Cell*. 15:773–780. doi:10.1016/j.devcel.2008.10.004

Mellitzer, G., Q. Xu, and D.G. Wilkinson. 1999. Eph receptors and ephrins restrict cell intermingling and communication. *Nature*. 400:77–81. doi:10.1038/21907

Nusse, R. 2008. Wnt signaling and stem cell control. *Cell Res.* 18:523–527. doi:10.1038/cr.2008.47

Park, H.C., C.H. Kim, Y.K. Bae, S.Y. Yeo, S.H. Kim, S.K. Hong, J. Shin, K.W. Yoo, M. Hibi, T. Hirano, et al. 2000. Analysis of upstream elements in the HuC promoter leads to the establishment of transgenic zebrafish with fluorescent neurons. *Dev. Biol.* 227:279–293. doi:10.1006/dbio.2000.9898

Rauch, G.J., M. Hammerschmidt, P. Blader, H.E. Schauerte, U. Strähle, P.W. Ingham, A.P. McMahon, and P. Haffter. 1997. Wnt5 is required for tail formation in the zebrafish embryo. *Cold Spring Harb. Symp. Quant. Biol.* 62:227–234.

Rohde, L.A., and C.-P. Heisenberg. 2007. Zebrafish gastrulation: cell movements, signals, and mechanisms. *Int. Rev. Cytol.* 261:159–192. doi:10.1016/S0074-7696(07)61004-3

Schambony, A., and D. Wedlich. 2007. Wnt-5A/Ror2 regulate expression of XPAPC through an alternative noncanonical signaling pathway. *Dev. Cell.* 12:779–792. doi:10.1016/j.devcel.2007.02.016

Schmitt, A.M., J. Shi, A.M. Wolf, C.C. Lu, L.A. King, and Y. Zou. 2006. Wnt-Ryk signalling mediates medial-lateral retinotectal topographic mapping. *Nature*. 439:31–37.

Simons, M., and M. Mlodzik. 2008. Planar cell polarity signaling: from fly development to human disease. *Annu. Rev. Genet.* 42:517–540. doi:10.1146/annurev.genet.42.110807.091432

Slusarski, D.C., and V.G. Corces. 2000. Calcium imaging in cell-cell signaling. *Methods Mol. Biol.* 135:253–261.

Slusarski, D.C., V.G. Corces, and R.T. Moon. 1997a. Interaction of Wnt and a Frizzled homologue triggers G-protein-linked phosphatidylinositol signalling. *Nature*. 390:410–413. doi:10.1038/37138

Slusarski, D.C., J. Yang-Snyder, W.B. Busa, and R.T. Moon. 1997b. Modulation of embryonic intracellular Ca2+ signaling by Wnt-5A. *Dev. Biol.* 182:114–120. doi:10.1006/dbio.1996.8463

Solnica-Krezel, L. 2005. Conserved patterns of cell movements during vertebrate gastrulation. *Curr. Biol.* 15:R213–R228. doi:10.1016/j.cub.2005.03.016

Stoick-Cooper, C.L., G. Weidinger, K.J. Riehle, C. Hubbert, M.B. Major, N. Fausto, and R.T. Moon. 2007. Distinct Wnt signaling pathways have opposing roles in appendage regeneration. *Development*. 134:479–489. doi:10.1242/dev.001123

van Amerongen, R., A. Mikels, and R. Nusse. 2008. Alternative wnt signaling is initiated by distinct receptors. *Sci. Signal.* 1:re9. doi:10.1126/scisignal.135re9

von der Hardt, S., J. Bakkers, A. Inbal, L. Carvalho, L. Solnica-Krezel, C.P. Heisenberg, and M. Hammerschmidt. 2007. The Bmp gradient of the zebrafish gastrula guides migrating lateral cells by regulating cell-cell adhesion. *Curr. Biol.* 17:475–487. doi:10.1016/j.cub.2007.02.013

Watanabe, A., S. Akita, N.T. Tin, N. Natsume, Y. Nakano, N. Niikawa, T. Uchiyama, and K. Yoshiura. 2006. A mutation in RYK is a genetic factor for nonsyndromic cleft lip and palate. *Cleft Palate Craniofac. J.* 43:310–316.

Westfall, T.A., R. Brimeyer, J. Twedt, J. Gladon, A. Olberding, M. Furutani-Seiki, and D.C. Slusarski. 2003a. Wnt-5/*pipetail* functions in vertebrate axis formation as a negative regulator of Wnt/β-catenin activity. *J. Cell Biol.* 162:889–898. doi:10.1083/jcb.200303107

Westfall, T.A., B. Hjertos, and D.C. Slusarski. 2003b. Requirement for intracellular calcium modulation in zebrafish dorsal-ventral patterning. *Dev. Biol.* 259:380–391. doi:10.1016/S0012-1606(03)00209-4

Witzel, S., V. Zimyanin, F. Carreira-Barbosa, M. Tada, and C.P. Heisenberg. 2006. Wnt11 controls cell contact persistence by local accumulation of Frizzled 7 at the plasma membrane. *J. Cell Biol.* 175:791–802. doi:10.1083/jcb.200606017

Wouda, R.R., M.R. Bansraj, A.W. de Jong, J.N. Noordermeer, and L.G. Fradkin. 2008. Src family kinases are required for WNT5 signaling through the Derailed/RYK receptor in the *Drosophila* embryonic central nervous system. *Development*. 135:2277–2287. doi:10.1242/dev.017319

Yamaguchi, T.P., A. Bradley, A.P. McMahon, and S. Jones. 1999. A Wnt5a pathway underlies outgrowth of multiple structures in the vertebrate embryo. *Development*. 126:1211–1223.

Yin, C., M. Kiskowski, P.A. Pouille, E. Farge, and L. Solnica-Krezel. 2008. Cooperation of polarized cell intercalations drives convergence and extension of presomitic mesoderm during zebrafish gastrulation. *J. Cell Biol.* 180:221–232. doi:10.1083/jcb.200704150

Yoshikawa, S., J.L. Bonkowsky, M. Kokel, S. Shyn, and J.B. Thomas. 2001. The derailed guidance receptor does not require kinase activity in vivo. *J. Neurosci.* 21:RC119.

Yoshikawa, S., R.D. McKinnon, M. Kokel, and J.B. Thomas. 2003. Wnt-mediated axon guidance via the *Drosophila* Derailed receptor. *Nature*. 422:583–588. doi:10.1038/nature01522

Zallen, J.A. 2007. Planar polarity and tissue morphogenesis. *Cell*. 129:1051–1063. doi:10.1016/j.cell.2007.05.050